

SANDIA REPORT

SAND2011-0564

Unlimited Release

February 2011

Assessing the Operational Life of Flexible Printed Boards Intended for Continuous Flexing Applications —a Case Study

David F. Beck

Prepared by
Sandia National Laboratories
Albuquerque, New Mexico 87185 and Livermore, California 94550

Sandia National Laboratories is a multi-program laboratory managed and operated by Sandia Corporation, a wholly owned subsidiary of Lockheed Martin Corporation, for the U.S. Department of Energy's National Nuclear Security Administration under contract DE-AC04-94AL85000.

Approved for public release; further dissemination unlimited.



Issued by Sandia National Laboratories, operated for the United States Department of Energy by Sandia Corporation.

NOTICE: This report was prepared as an account of work sponsored by an agency of the United States Government. Neither the United States Government, nor any agency thereof, nor any of their employees, nor any of their contractors, subcontractors, or their employees, make any warranty, express or implied, or assume any legal liability or responsibility for the accuracy, completeness, or usefulness of any information, apparatus, product, or process disclosed, or represent that its use would not infringe privately owned rights. Reference herein to any specific commercial product, process, or service by trade name, trademark, manufacturer, or otherwise, does not necessarily constitute or imply its endorsement, recommendation, or favoring by the United States Government, any agency thereof, or any of their contractors or subcontractors. The views and opinions expressed herein do not necessarily state or reflect those of the United States Government, any agency thereof, or any of their contractors.

Printed in the United States of America. This report has been reproduced directly from the best available copy.

Available to DOE and DOE contractors from
U.S. Department of Energy
Office of Scientific and Technical Information
P.O. Box 62
Oak Ridge, TN 37831

Telephone: (865) 576-8401
Facsimile: (865) 576-5728
E-Mail: reports@adonis.osti.gov
Online ordering: <http://www.osti.gov/bridge>

Available to the public from
U.S. Department of Commerce
National Technical Information Service
5285 Port Royal Rd.
Springfield, VA 22161

Telephone: (800) 553-6847
Facsimile: (703) 605-6900
E-Mail: orders@ntis.fedworld.gov
Online order: <http://www.ntis.gov/help/ordermethods.asp?loc=7-4-0#online>



SAND2011-0564

Unlimited Release

February 2011

Assessing the Operational Life of Flexible Printed Boards Intended for Continuous Flexing Applications —a Case Study

David F. Beck
Hard Target Systems
Sandia National Laboratories
P.O. Box 5800
Albuquerque, New Mexico 87185-MS0530

Abstract

Through the vehicle of a case study, this paper describes in detail how the guidance found in the suite of IPC (Association Connecting Electronics Industries) publications can be applied to develop a high level of design assurance that flexible printed boards intended for continuous flexing applications will satisfy specified lifetime requirements.

CONTENTS

1	Introduction	9
2	Flexibility Assessment	11
2.1	Strain Model	12
2.1.1	Configuration geometry	12
2.1.2	Number of Flexures.....	29
2.1.3	Maximum strain-range calculations	33
2.1.4	Strain-range distributions.....	36
2.2	Ductility Model.....	41
2.2.1	Materials selection.....	41
2.2.2	Conductor Ductility	44
2.2.3	Design Ductility.....	48
2.3	Design-life Assessment.....	57
2.3.1	Cable strain-range spectra	57
2.3.2	Flexibility Assessment	59
2.4	Design Change Options to Achieve Desired Life.....	59
2.4.1	Alternate Configuration.....	59
2.4.2	Larger Bend Radius.....	61
2.4.3	Increase Ductility	61
3	Cable Qualification	63

FIGURES

Figure 1.	Flexible printed circuit design decision logic (IPC-D-330 Figure 7-64).	11
Figure 2.	Two-dimensional cross-section of a conceptual basic flat cable (not to scale).	12
Figure 3.	Flat cable and sub-cable material stack ups.	14
Figure 4.	C27-4 material stack up (SEM on left; P/N details subject to correction).	14
Figure 5.	Illustration of flat cable layout.	16

Figure 6. Flat cable conductor trace patterns.....	17
Figure 7. Flat cable installation configuration.....	20
Figure 8. Bending the omega section of a flat cable into the installed geometry (C28 cable shown).....	21
Figure 9. Simplified omega-flex circuit loading diagram.....	21
Figure 10. Prototype C27 and C28 cable bundles installed in fit-check fixtures illustrating the general twisting behavior found in the “legs” of the loop.	22
Figure 11. Illustration of reduced bend radii in flat cable folds.....	24
Figure 12. Illustration of fold cross-section location and curvature projection.....	26
Figure 13. Sectional view of flex cable fold cross-section (see Figure 12).....	26
Figure 14. Flex cable fold radius of curvature behavior.....	28
Figure 15. “Day-in-the-life” telescope gimbal re-points.	30
Figure 16. Gimbal positions for one-third of a day-in-the-life.	31
Figure 17. Gimbal positions for one simulated day-in-the-life.....	32
Figure 18. Simplified day-in-the-life elevation and azimuth pointing model.	32
Figure 19. Nomenclature for layer stress analysis (from IPC-2223 Figure 5-7).	33
Figure 20. Strain-rate model.	36
Figure 21. Example omega-flex cable strain profile for point originating at fold apex (C28-3 layer 2 outer trace edge shown).....	37
Figure 22. C28-3 layer 2 strains and strain-range distributions.....	38
Figure 23. Maximum strain-range cumulative distributions for the omega flex cables. ..	39
Figure 24. Prototypic test evidence in support of strain model.	40
Figure 25. Representative SEM views of a copper foil cross section and surfaces.....	42
Figure 26. Ductility results for high temperature ductility electrodeposited copper foil, CF-E3, for various weights and foil vendors (IPC-TR-484 Figure 12).....	44

Figure 27. Weibull cumulative density plot of copper foil sample fatigue data.....	46
Figure 28. Ductility results for electrodeposited copper foil in use by the cable vendor.	47
Figure 29. Coffin-Manson plot illustrating built-up cable (“pseudocircuit”) fatigue performance relative to bare copper foil.....	49
Figure 30. Copper foil fatigue data illustrating anneal temperature effects on ductility..	49
Figure 31. Reduction in available ductility due to conductor defects.....	50
Figure 32. Typical test coupon used to develop flex cable fatigue design envelope.....	51
Figure 33. IPC-TM-650 Method 2.4.3.1 tester with installed cable sample.....	52
Figure 34. Vendor fixture used for conducting cable endurance testing.....	52
Figure 35. Omega flex cable design ductility model.....	53
Figure 36. Prototype C27-4 cable fatigue damage model.....	56
Figure 37. Strain-range spectra for the original 2-oz flex cables.....	58
Figure 38. Strain-range spectra for the original 3-oz flex cables.....	58
Figure 39. Strain-range spectra for the 2-oz omega flex cables with the redesigned C27-4 and C28-2.....	60
Figure 40. Strain-range spectra for the 3-oz omega flex cables under the new constraints set by the redesigned C27-4 cable.....	60
Figure 41. C27 cable set load spectra for 3-oz, double-layer C27-4 design.....	61

TABLES

Table 1. List of Flat Cable Fabrication Drawings Used in the Assessment	13
Table 2. Flat Cable Thickness.....	15
Table 3. Flat Cable Conductor Trace Widths	17
Table 4. Flat Cable Conductor Pattern Width (\pm From Omega Centerline).....	19

Table 5. Omega Cable Constraining Surface Separation or Standoff Distance	23
Table 6. Omega Cable Apex Bend Radii (Inner Side).....	24
Table 7. Maximum Strain Range Calculations.....	35
Table 8. Copper Materials Selected for use in the Original Cable Build	43
Table 9. Omega Flex Cable Design Limit Fit Summary	55

1 Introduction

This paper is intended to describe a method for assessing the design life of flat cables used in continuous flexing applications in sufficient detail that it can be readily adapted and used by designers for their particular applications. The method is presented in the form of a case study for two sets of cables that were used to carry electrical signals and power across articulated joints in a telescope, where they were subject to repeated flexural loads as the gimbaled telescope was slewed to point in different directions. Furthermore, it should be noted that the requirements to be met included an operational design life of ten years. The cable bundle associated with the azimuth axis of the telescope has been assigned the designator C27, while the bundle crossing the elevation axis is designated C28; suffixes will be used to designate particular cables within a bundle.

From the outset the intent was to use an accepted, design standard. The only, currently-active candidate identified for flex cable design is IPC-2223, *Sectional Design Standard for Flexible Printed Boards*, which was adopted on 01SEP99 for use by the Department of Defense. In turn, IPC-2223 includes, by reference, a number of other standards, of which IPC-MF-150, *Metal Foil for Printed Wiring Applications* is important from a flexibility design standpoint. IPC-MF-150 itself was superseded by IPC-4562 in May 2000 (same title). In its turn, also by reference, IPC-4562 includes (as IPC-MF-150 before) IPC-D-330, *Design Guide Manual*, and IPC-TR-484, *Results of Copper Foil Ductility Round Robin*. This suite of IPC (Association Connecting Electronics Industries) publications formed the basis of the flat cable flexibility assessment provided below.

2 Flexibility Assessment

IPC-D-300 §7 includes an example decision diagram intended for use in assessing design concepts vis-à-vis flexibility requirements. As it is useful for following the assessment documented herein, it is reproduced below as Figure 1, with annotations pointing to the applicable sections of this report.

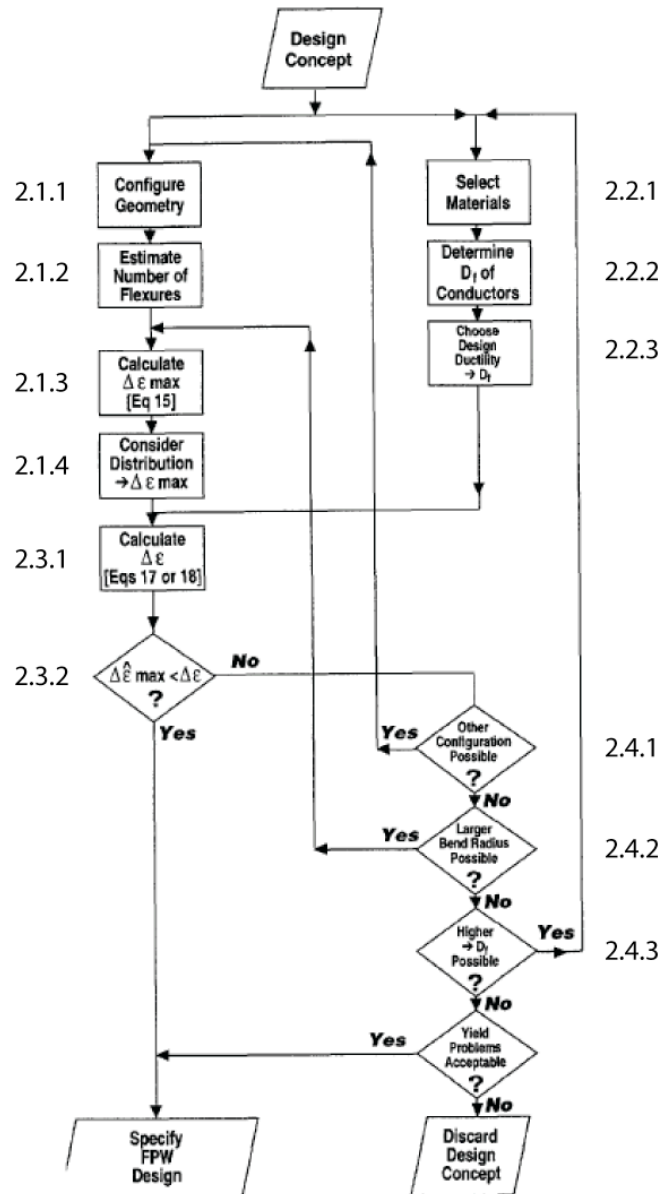


Figure 1. Flexible printed circuit design decision logic (IPC-D-330 Figure 7-64).

2.1 Strain Model

2.1.1 Configuration geometry

A basic flexible flat cable (flexible printed circuit board) consists of a material stack up of multiple foils, sheets, films, and fabrics that serve as conductors, dielectrics (insulators and adhesives), and shields. The conductor material in the cables of concern here is etched, electrodeposited copper foil of varying weight, specified as 1-, 2-, or 3-oz per square foot per IPC-4562 (nominal thickness of 1.35, 2.70, or 4.05 mils respectively). The cable insulation is provided by DuPont Kapton[®] polyimide film that meets ASTM D 5213. The shield material in use is a 400-mesh, phosphor-bronze, plain-weave screen or fabric, of 0.0010-inch diameter wire; seams of the shield are spot welded (0.400-inch minimum overlap of fabric edges with welds every one-half inch maximum (one-quarter inch typical)). The cable adhesive that bonds the resulting stack-up of conductors, insulation, and shields together is DuPont Teflon[®] FEP (fluorinated ethylene propylene). A conceptual sketch of the two-dimensional cross-section of a basic flat cable is provided in Figure 2.

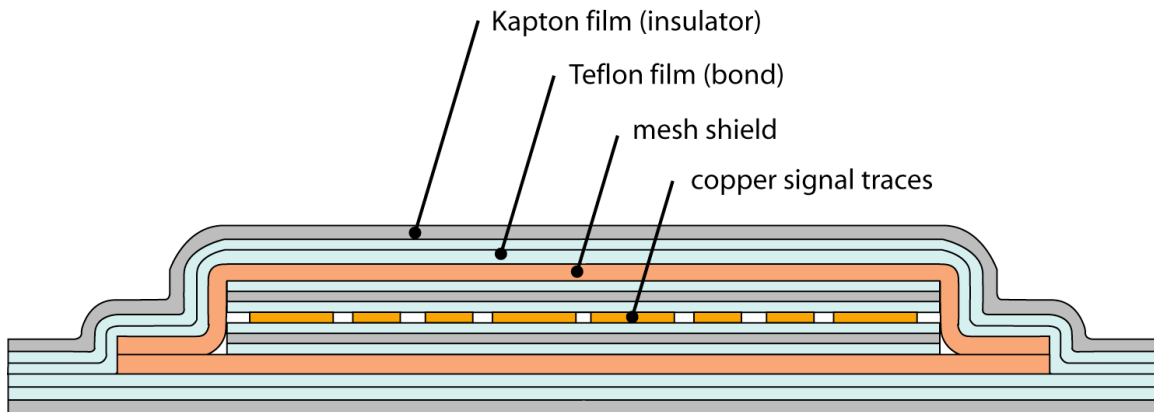


Figure 2. Two-dimensional cross-section of a conceptual basic flat cable (not to scale).

In the current application, an actual, connectorized cable may contain from one to three of these bonded stack-ups. In addition to using cables with a single layer of copper conductors (as in Figure 2), the several flat cable designs also make use of bonded stack-

ups that include two layers¹ of copper (these two different stack ups may also be referred to as single-sided circuits or double-sided circuits in keeping with IPC-2223).

The stack up of basic materials within the flat cables was partially summarized in the cable fabrication drawings (although note that the thicknesses given were representative only); these drawings are listed for reference purposes in Table 1. A one-dimensional cross-section for each of the flat cables is provided in Figure 3 that illustrates the actual bonded stack-ups forming each sub-cable and cable by designator. Note that the actual stack up by material part number was not, unfortunately, defined in the drawings; however, a likely configuration—based on the set of material certifications provided by the cable vendor—is provided in Figure 4.

Table 1. List of Flat Cable Fabrication Drawings Used in the Assessment

Drawing	Description
R75996	Azimuth Flex Cable C27-1 EL Data
R75997	Azimuth Flex Cable C27-2 ARS
R75998	Azimuth Flex Cable C27-3 EL Motor Pwr.
R75999	Azimuth Flex Cable C27-4 GNET
R75967	Azimuth Flex Cable C27-5 Analog
R76728	Elevation Cable 28-1 Analog Sig. Fab.
R76730	Elevation Cable 28-2 G-NET Signals Fab.
R76729	Elevation Cable 28-3 EL ARS Fab.

¹ It should be noted that “layer” is an overloaded term often found in project documentation related to flex cables and is variously applied to: (1) the individual sheets or films of conductors, dielectric materials, and shields in a stack-up; (2) an individual bonded stack-up in a sub-cable; and (3), in reference to the particular number of conductor sheets, films, or traces in a stack-up, as here (i.e., single or double layer of copper conductors).

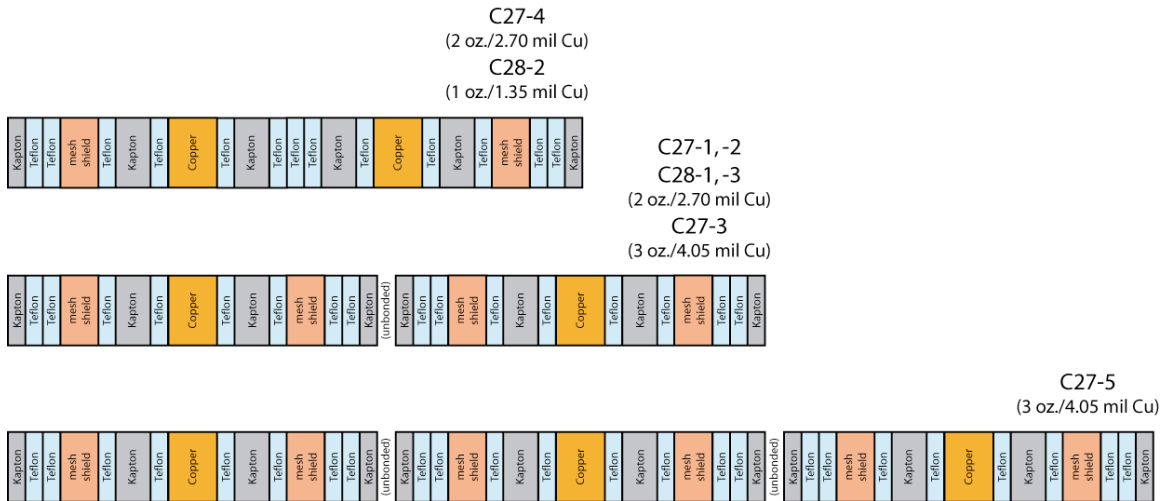


Figure 3. Flat cable and sub-cable material stack ups.

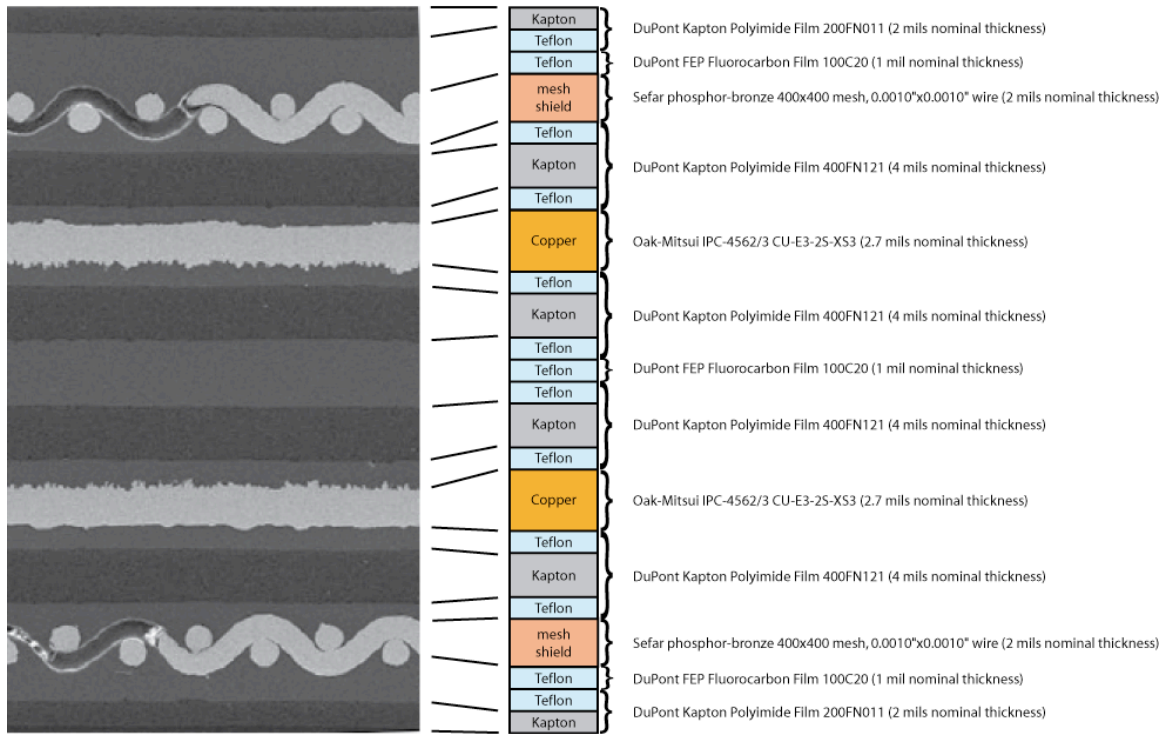


Figure 4. C27-4 material stack up (SEM on left; P/N details subject to correction).

From the data found in Figure 4 it might be expected that, as an example, the nominal C27-4 cable thickness would be 32.4 mils. However, due to Kapton and Teflon shrinkage (something on the order of 0.1 to 1 % based on DuPont datasheets), and due to Teflon “flowing” into the voids in the shield mesh and enhanced bond surfaces of the copper conductors (as part of the cable manufacturing process), the final C27-4 cable thickness is

actually on the order of 29 to 30 mils (based on an uncontrolled sampling of an available spare cable and use of an un-calibrated micrometer). In comparison, the maximum thickness of a single 2-oz copper layer bonded stack-up is 0.020 inches.² Based on thicknesses observed in two SEM cross sections, the nominal flat cable cover layer thickness (Kapton and Teflon) is 7.7 mils (the average of nine measurements taken that ranged from 7.3 to 8.3 mils; compare to 9 mils nominal thickness), while the nominal base layer thickness (Kapton and Teflon material between the two-copper-layer C27-4 and C28-2 designs) is 8.9 mils (the average of five measurements taken that ranged from 8.3 to 9.5 mils; compare to 9 mils nominal thickness). The available DuPont datasheets do not provide information on thickness variations in the Kapton or Teflon films used. No datasheets were found to describe the shield material beyond the description given earlier. The tolerance in electrodeposited foil thickness is $\pm 10\%$ per IPC-4562. These data can be compiled to provide a cable thickness “model”, as in Table 2 below.

Table 2. Flat Cable Thickness

Cable Layer	oz.	t_{min} (in)	t_{nom} (in)	t_{max} (in)
C28-1 layer 1	2	0.0170	0.0181	0.0196
C28-1 layer 2	2	0.0170	0.0181	0.0196
C28-2 (double CU)	1	0.0253	0.0270	0.0291
C28-3 layer 1	2	0.0170	0.0181	0.0196
C28-3 layer 2	2	0.0170	0.0181	0.0196
C27-1 layer 1	2	0.0170	0.0181	0.0196
C27-1 layer 2	2	0.0170	0.0181	0.0196
C27-2 layer 1	2	0.0170	0.0181	0.0196
C27-2 layer 2	2	0.0170	0.0181	0.0196
C27-3 layer 1	3	0.0182	0.0195	0.0211
C27-3 layer 2	3	0.0182	0.0195	0.0211
C27-4 (double CU)	2	0.0278	0.0297	0.0320
C27-5 layer 1	3	0.0182	0.0195	0.0211
C27-5 layer 2	3	0.0182	0.0195	0.0211
C27-5 layer 3	3	0.0182	0.0195	0.0211

An illustration of the layout of the two basic types of flat cables (C27 and C28) is provided in Figure 5. The section of the cables subject to dynamic flexing is the omega-like or circular portion of the cable. For reference, the radius of the C28 omega centerline

² Cable vendor, *Cable Construction*, Drawing No. 1943-7, Rev. B.

is 2.07 inches, while that of a C27 cable is 5.13 inches (2.88-inch ID/5.38-inch OD and 9.00-inch ID/11.50-inch OD respectively;³ cable width 1.25 ±0.03).

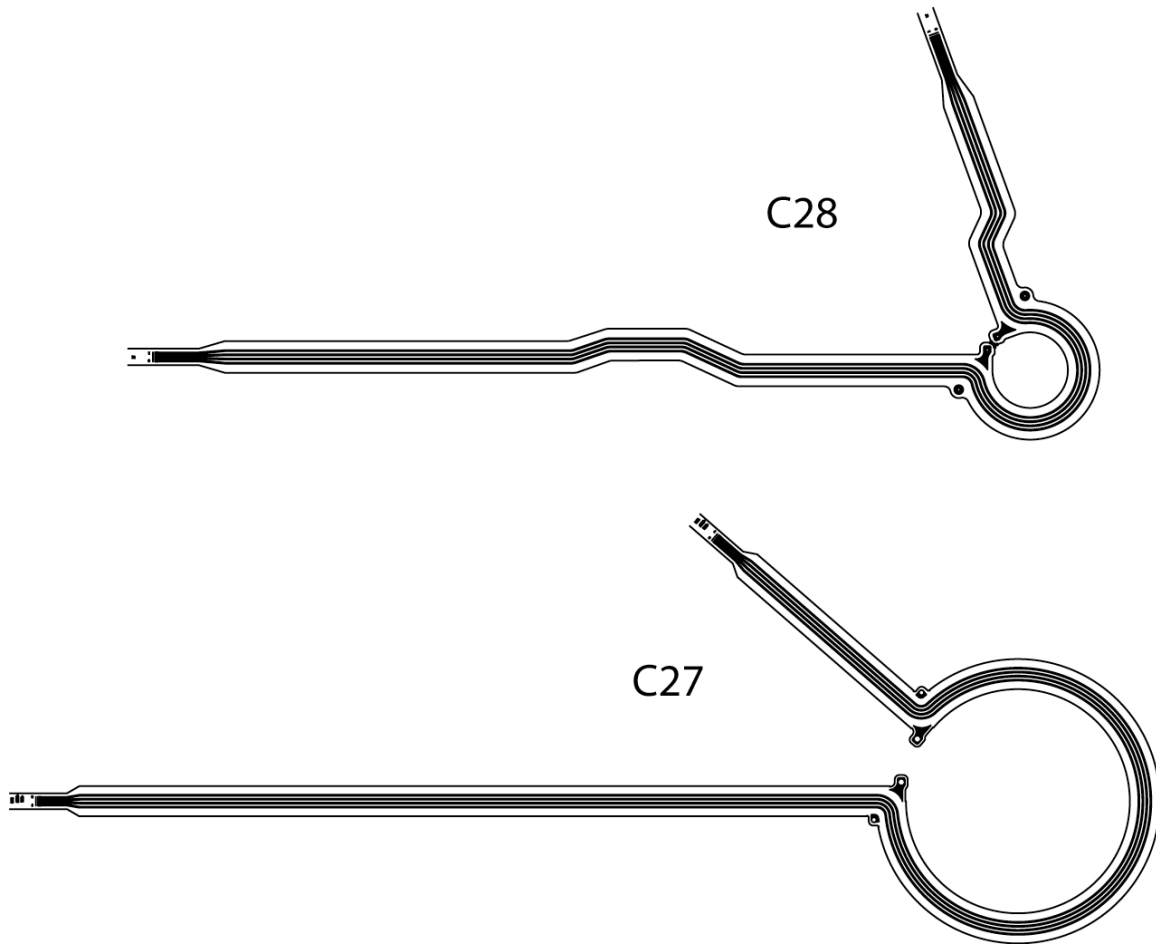


Figure 5. Illustration of flat cable layout.

Conductor trace patterns across the set of flat cables vary considerably between the different bonded stack ups involved. The importance of trace size and position in a cable in regards to strain will be enumerated further below. The trace patterns for the existing cable designs are illustrated in Figure 6 (the patterns are indexed by the trailing digits of the cable vendor's drawing number). Individual trace widths are summarized in Table 3

³ No tolerances are specified on these radii on the manufacturer's cable assembly drawings. The cable fabrication drawings imply ± 0.03 inches.

(per drawings, except patterns 203-2 and 212-2 which are based on measurements of artwork drawings).

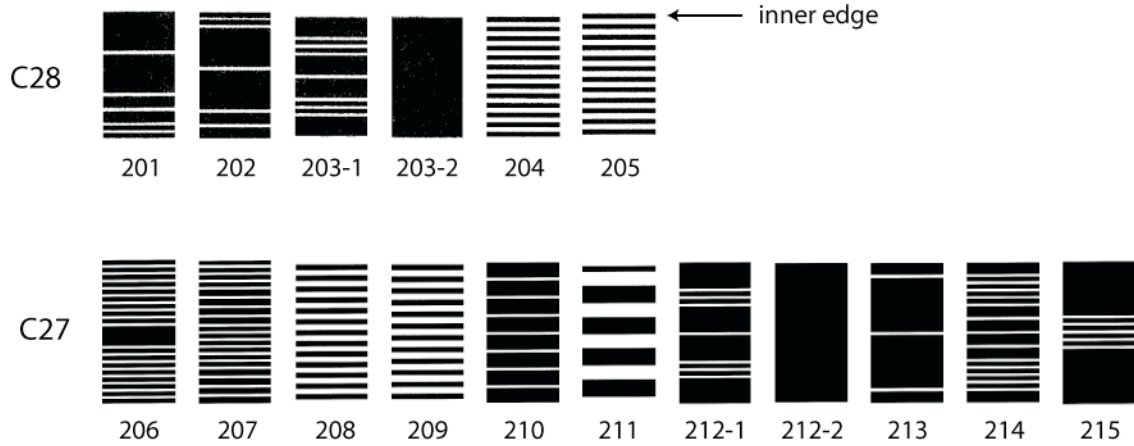


Figure 6. Flat cable conductor trace patterns.

Table 3. Flat Cable Conductor Trace Widths

Cable Layer	pattern no.	oz.	trace width (inches)																
			0.020	0.025	0.030	0.035	0.040	0.045	0.060	0.085	0.090	0.105	0.140	0.147	0.190	0.285	0.380	0.860	0.998
C28-1 layer 1	201	2				X										X			
C28-1 layer 2	202	2				X										X			
C28-2 "layer" 1	203-1	1	X										X						
C28-2 "layer" 2	203-2	1																X	
C28-3 layer 1	204	2				X													
C28-3 layer 2	205	2				X													
C27-1 layer 1	206	2			X							X							
C27-1 layer 2	207	2			X		X	X	X										
C27-2 layer 1	208	2				X													
C27-2 layer 2	209	2				X													
C27-3 layer 1	210	3										X							
C27-3 layer 2	211	3				X						X							
C27-4 "layer" 1	212-1	2	X												X				
C27-4 "layer" 2	212-2	2																	X
C27-5 layer 1	213	3										X					X		
C27-5 layer 2	214	3		X								X	X						
C27-5 layer 3	215	3			X												X		

From a strain perspective, it is important to note the differences between patterns 203-1 and 203-2 in C28-2, and between 212-1 and 212-2 in C27-4. IPC-D-330 §7.11.4 states that “the designer should follow these prudent design rules as a matter of good design

practice: ... Conductor patterns on both sides of double-sided flexible printed circuit should be essentially identical.” IPC-2223 §5.2.3.3 states, however, “For maximum dynamic flex life...conductors in the bend area...should adhere to the following considerations: ...Conductors in double-sided circuits should not be placed directly over each other, which produces an “I” beam effect.” Unfortunately the design of C27-4 and C28-2 does not follow the guidance of either reference. The ground planes (203-2 and 212-2) will be stiffer than the signal traces, and the resulting shift in the neutral surfaces will cause the signal layer conductor traces to experience greater strains than if a balanced design had been implemented. This shift in the neutral surface in C27-4 and C28-2 will require appropriate consideration when estimating strains.

Understanding the conductor patterns of these flat cables is also important in identifying bounding strain locations (or expected failure locations for a given fatigue strain range). Narrow trace widths are expected to exhibit reduced flex lives relative to wider traces. This is due to consideration of flaw-size-to-conductor-width ratios, crack propagation times, and strain relief possibilities.⁴ As a practical example, again consider C27-4 and C28-2; even if the design had been balanced such that the ground planes and signal traces were subject to the same strain magnitudes, it would be expected that failures would occur first on the signal traces.

Finally, because the strain field in a cable will be a function of radial position, it is necessary to have an understanding of the trace positions within each cable. For bounding analyses, only the outer edges of the trace patterns are actually required; for this purpose trace pattern widths for each sub-cable (relative to the omega centerline) are given in Table 4 (based on artwork measurements).

⁴ IPC-TM-650 Method 2.4.3.1 §3.2.

Table 4. Flat Cable Conductor Pattern Width (\pm From Omega Centerline)

Cable Layer	pattern no.	trace pattern half-width (inches)
C28-1 layer 1	201	0.45
C28-1 layer 2	202	0.45
C28-2 "layer" 1	203-1	0.43
C28-2 "layer" 2	203-2	0.43
C28-3 layer 1	204	0.43
C28-3 layer 2	205	0.44
C27-1 layer 1	206	0.541
C27-1 layer 2	207	0.544
C27-2 layer 1	208	0.445
C27-2 layer 2	209	0.445
C27-3 layer 1	210	0.509
C27-3 layer 2	211	0.435
C27-4 "layer" 1	212-1	0.519
C27-4 "layer" 2	212-2	0.499
C27-5 layer 1	213	0.504
C27-5 layer 2	214	0.524
C27-5 layer 3	215	0.509

The set of three C28-X cables (five bonded layer stack ups using the double-sided C28-2) form the C28 cable bundle. The stacking order “bottom-to-top” is C28-2, C28-1, and C28-3 (by trace pattern: 203-2, 203-1, 202, 201, 204, and 205). Likewise, the C27 cable bundle ordering (with the double-sided C27-4) is C27-1, C27-2, C27-3, C27-4, and C27-5 (by trace pattern: 207, 206, 209, 208, 211, 210, 212-2, 212-1, 215, 214, and 213).

While the C27 and C28 cables are built flat following the illustration of Figure 5, the as-installed geometry is quite complex, as illustrated in Figure 7 below. The dimensions (e.g., nominal bend radius) of the flexing portions of the flat cables are governed by the surrounding mechanical assemblies⁵ and adjacent flex cables. The resulting nominal mechanical assembly dimensions stack up to constrain the outer sides of the folded C27 cable set to 2.612 inches, and C28 to 2.361 inches (ICDs 3024 and 2576 are in error).

⁵ Applicable drawings are: for C27, 3168, 3169, 1663, 1617, and 3219; for C28, 3165, 2203, 3158, 3159, 1653, 3038, 3201, 1654, and 3166.

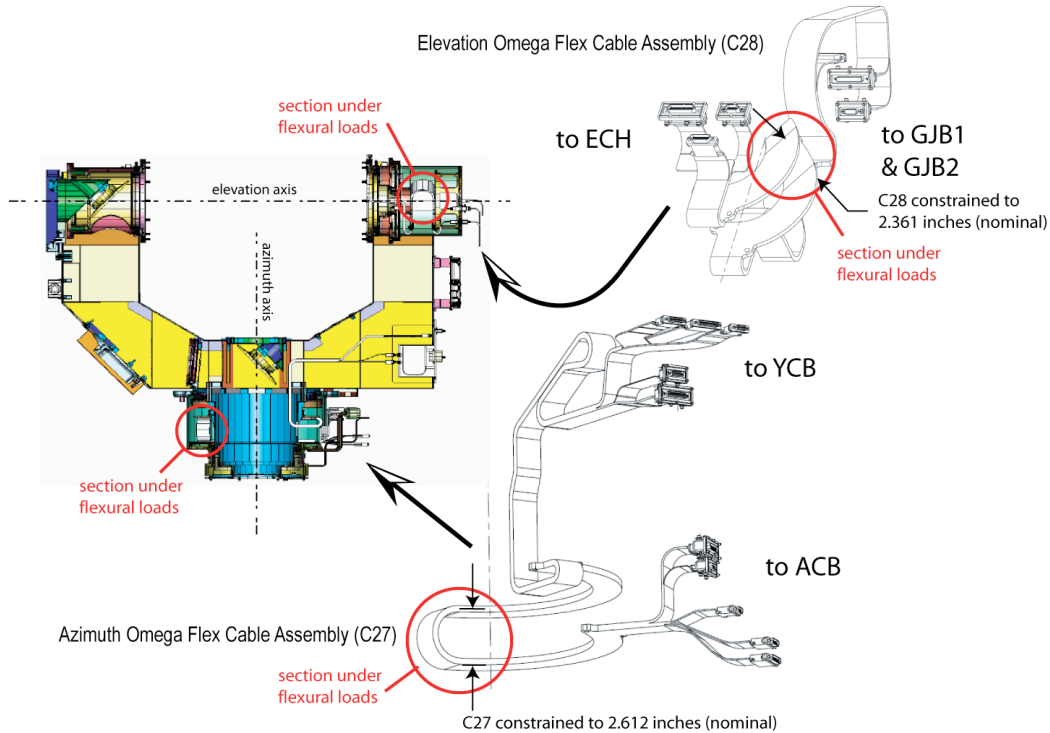


Figure 7. Flat cable installation configuration.

Because the cables exhibit a certain amount of stiffness, a torque has to be applied about the centerline of the omega section of the cables at the mounts in order to produce the required loop or fold, as illustrated in Figure 8. Away from the fold the cable responds to the torque by twisting,⁶ necessitating application of a compressive force to flatten these sections sufficiently to fit within the constraining geometry. The fold in the cable, and the twist in those portions of the cable leading up to the fold, can also be understood by considering the simplified—two-dimensional—static load diagram of Figure 9. The actual degree of twisting is related to cable stiffness and so to the strength of the end couples required to fold the cable, and thus it will vary somewhat between different layer stack ups. The observed response of the cable to the applied forces also varies with radial position and contact patterns (e.g., the twisting or departure away from the constraining plane is somewhat less along the inner edge of the omega than along the outer edge).

⁶I.e., the observed “wave” in the cable is not a buckle, which is a completely different phenomenon. However, if two cable layers interfere with each other in the fold region, any resulting buckling tendencies would likely be absorbed into the twist.

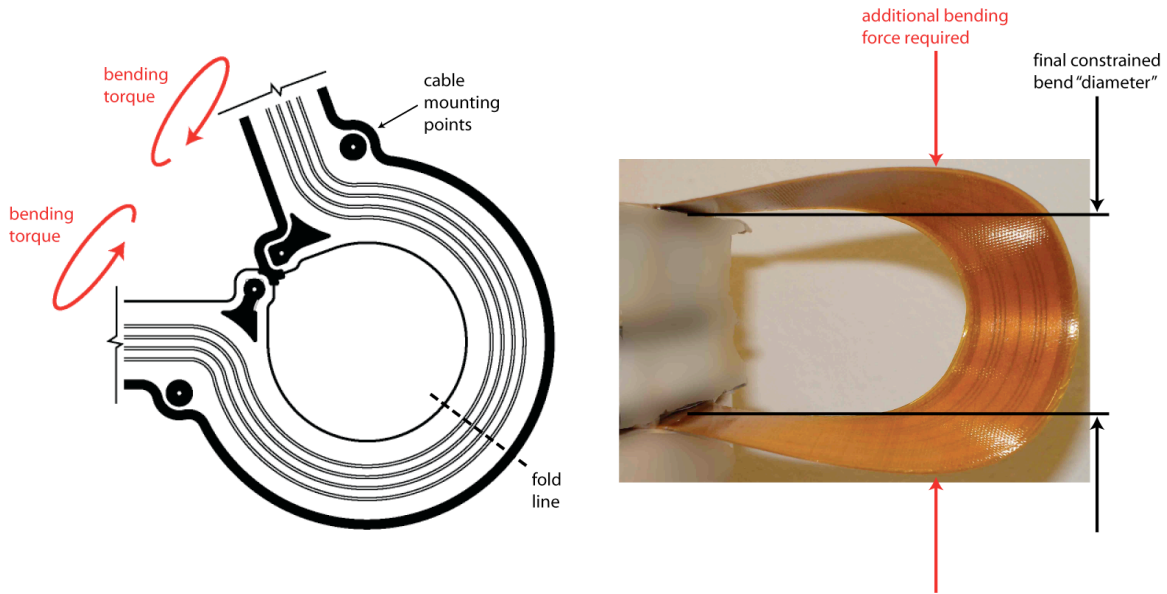


Figure 8. Bending the omega section of a flat cable into the installed geometry (C28 cable shown).

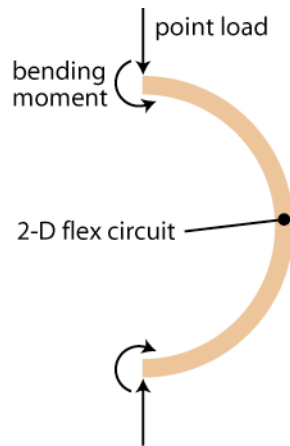


Figure 9. Simplified omega-flex circuit loading diagram.

The final behavior of the flat cable bundles, as installed, is illustrated in Figure 10. Note that the ordering of cables and layer stack ups from the outside (largest “diameter”) to the inside of the fold corresponds to the bottom-to-top ordering presented earlier; the resulting constraint dimensions (i.e., fold sizes), S , are provided in Table 5 (based on the cable thickness “model” of Table 2 and applicable mechanical drawings).

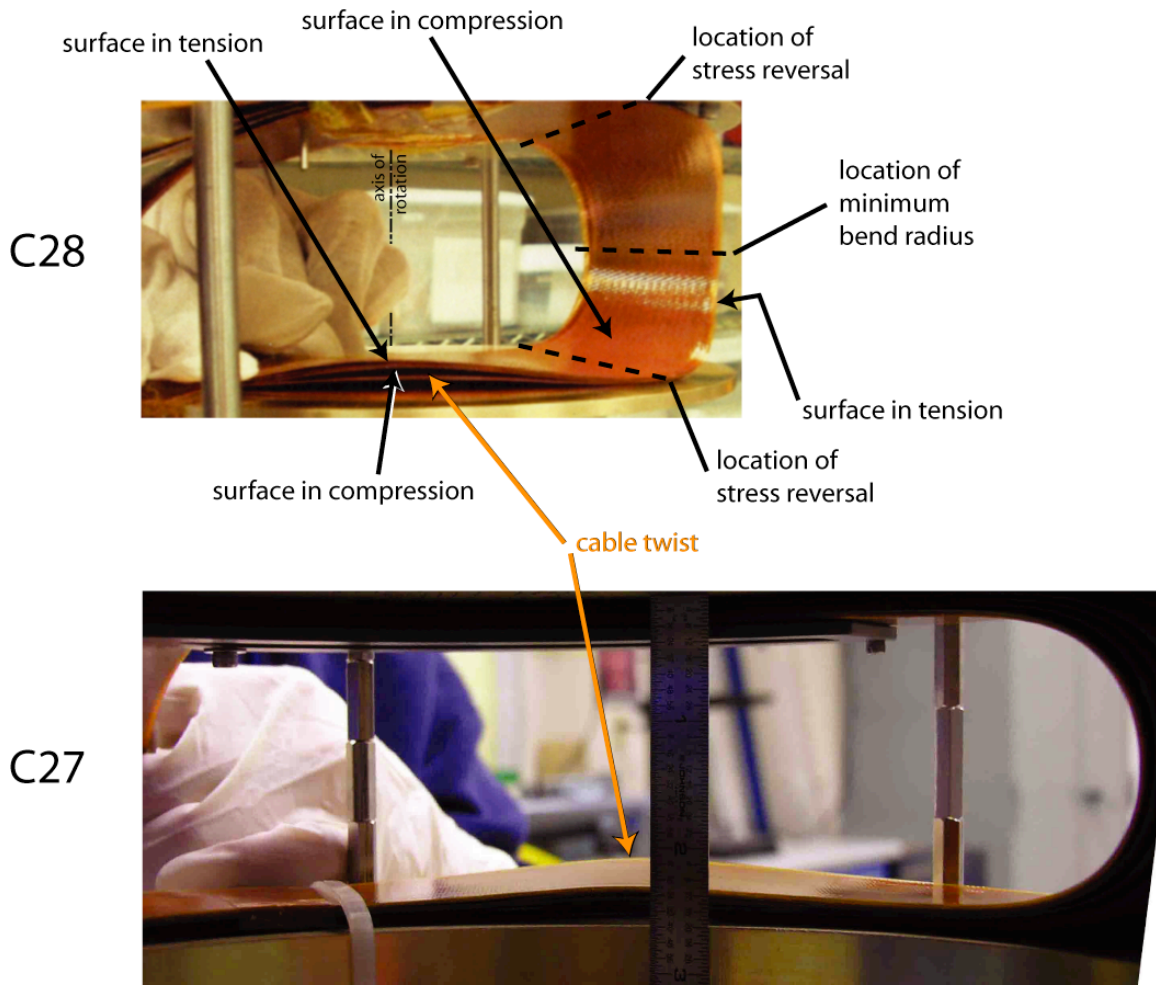


Figure 10. Prototype C27 and C28 cable bundles installed in fit-check fixtures illustrating the general twisting behavior found in the “legs” of the loop.

Table 5. Omega Cable Constraining Surface Separation or Standoff Distance⁷

Cable Layer	pattern no.	oz.	S_{min} (in)	S_{nom} (in)	S_{max} (in)
C28-2 (double CU)	203	1	2.259	2.361	2.402
C28-1 layer 2	202	2	2.201	2.307	2.351
C28-1 layer 1	201	2	2.162	2.271	2.317
C28-3 layer 1	204	2	2.123	2.235	2.283
C28-3 layer 2	205	2	2.083	2.198	2.249
C27-1 layer 2	207	2	2.573	2.612	2.656
C27-1 layer 1	206	2	2.534	2.576	2.622
C27-2 layer 2	209	2	2.495	2.540	2.588
C27-2 layer 1	208	2	2.456	2.503	2.554
C27-3 layer 2	211	3	2.416	2.467	2.520
C27-3 layer 1	210	3	2.374	2.428	2.483
C27-4 (double CU)	212	2	2.332	2.389	2.447
C27-5 layer 3	215	3	2.268	2.330	2.391
C27-5 layer 2	214	3	2.226	2.291	2.355
C27-5 layer 1	213	3	2.184	2.252	2.318

While it might seem reasonable at this point to assume that free-form (no mandrel) flexible printed circuit bend geometry is circular—i.e., to assume that the constrained dimensions of Table 5 provide the bend diameter of the loop—this is not the case. As pointed out in IPC-D-330 §7.11.1.4 (cf. §7.11.3.1):

A flexible printed circuit may be bent without the benefit of a forming mandrel. The resulting bend geometries are noncircular and have a minimum radius of curvature at the bend apex which is significantly smaller than the radius resulting from a circular bend in the same space.

Since later in this paper the maximum strains in the omega cables are to be estimated—which will occur at the apex of the fold—it is necessary to determine a “correction” factor. To this end several existing cable photographs of the fold area were digitally enhanced to clearly demarcate the cable edges, and the radius of the fold apex of each resulting image was estimated. The observed variation and departure from circular is illustrated in Figure 11. As the data could not be correlated with cable construction, and because the effects of camera perspective could not be accounted for, the observed reduction in apex radii from those expected based on the constraining dimensions (84%

⁷ C28-2 and C27-1 constraint dimensions are set by the surrounding mechanical assemblies.

to 90%, 87% average) will be treated as a random variable, ξ ; minimum, maximum, and average values were applied to the data of Table 2 and Table 5 to develop an estimate for the expected range of C27 and C28 cable fold apex bend radii, as found in Table 6.

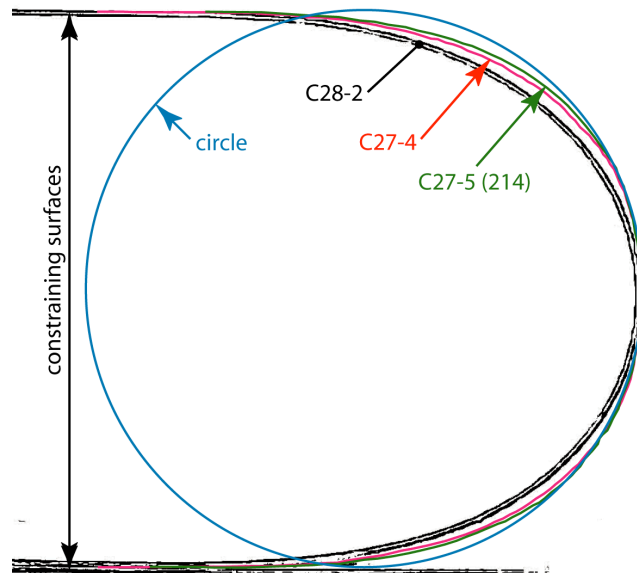


Figure 11. Illustration of reduced bend radii in flat cable folds.

Table 6. Omega Cable Apex Bend Radii (Inner Side)

Cable Layer	pattern no.	oz.	A_{min} (in)	A_{nom} (in)	A_{max} (in)
C28-2 (double CU)	203	1	0.924	1.004	1.058
C28-1 layer 2	202	2	0.908	0.988	1.043
C28-1 layer 1	201	2	0.891	0.972	1.027
C28-3 layer 1	204	2	0.875	0.956	1.012
C28-3 layer 2	205	2	0.859	0.941	0.997
C27-1 layer 2	207	2	1.064	1.120	1.180
C27-1 layer 1	206	2	1.048	1.105	1.165
C27-2 layer 2	209	2	1.031	1.089	1.149
C27-2 layer 1	208	2	1.015	1.073	1.134
C27-3 layer 2	211	3	0.997	1.056	1.117
C27-3 layer 1	210	3	0.980	1.039	1.101
C27-4 (double CU)	212	2	0.953	1.014	1.076
C27-5 layer 3	215	3	0.935	0.997	1.060
C27-5 layer 2	214	3	0.917	0.980	1.043
C27-5 layer 1	213	3	0.900	0.963	1.027

As part of the effort to assess the fatigue life of flex cables, it is necessary to characterize the expected strain-range. A first approximation can be made by simply assuming that the

worst case strain range is associated with movement of a point from the apex of the bend (point of maximum strain⁸) to a constraining surface (point of no strain). This should provide a conservative estimate⁹, as outlined here: operational slews¹⁰ in elevation and azimuth will be less than ± 15 degrees from the nadir (discussed in §2.1.3); that is, the maximum slew about either axis will be on the order of 30 degrees. Considering the outer edge of the widest trace patterns presented in Table 4, calculations using this slew yield a maximum circumferential travel along the cable of 0.66 inches for C28-1 and 1.48 inches for C27-1 layer 2 (travel along the inner traces of these cables and along all traces of other cables in the respective cable bundles will be less). The minimum fold dimensions from Table 5 can then be used to determine a minimal, conservative bound on the distance along the cable from the apex to a constraint by assuming that the folds form semicircles; the results so obtained are 1.8 inches for C28-1 and 2.0 inches for C27-1 layer 2. Comparison of these circumferential travel and apex-to-plate distances clearly indicates that the actual strain ranges will be less in magnitude than the maximum strain of the apex (i.e., conservative, as claimed above).

In order to develop a more refined estimate for the strain ranges of these cables, it is necessary to develop a model describing the geometry of the fold behind the apex. The approach taken here is to consider a cross-section of the fold—i.e., a cross-section that is perpendicular to the fold line—which can be projected onto the circuit traces and so support derivation of the strain at any point. This approach is illustrated in Figure 12. An edge-enhanced image of a photograph showing a representative cross-section of a fold is shown in Figure 13.

⁸ As determined using the data of Table 2 and Table 6.

⁹ Strain calculations are presented in §2.1.3.

¹⁰ Movements other than placing the telescope in a stow position.

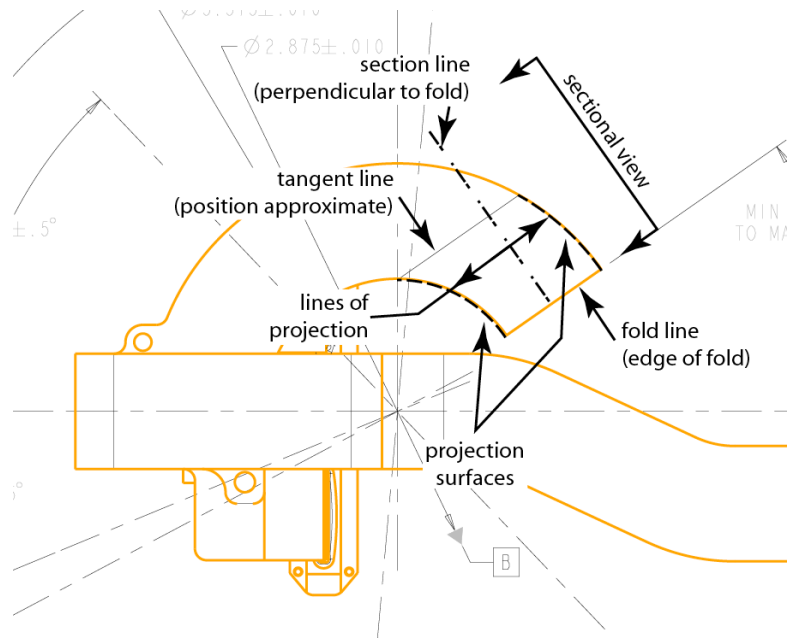


Figure 12. Illustration of fold cross-section location and curvature projection.

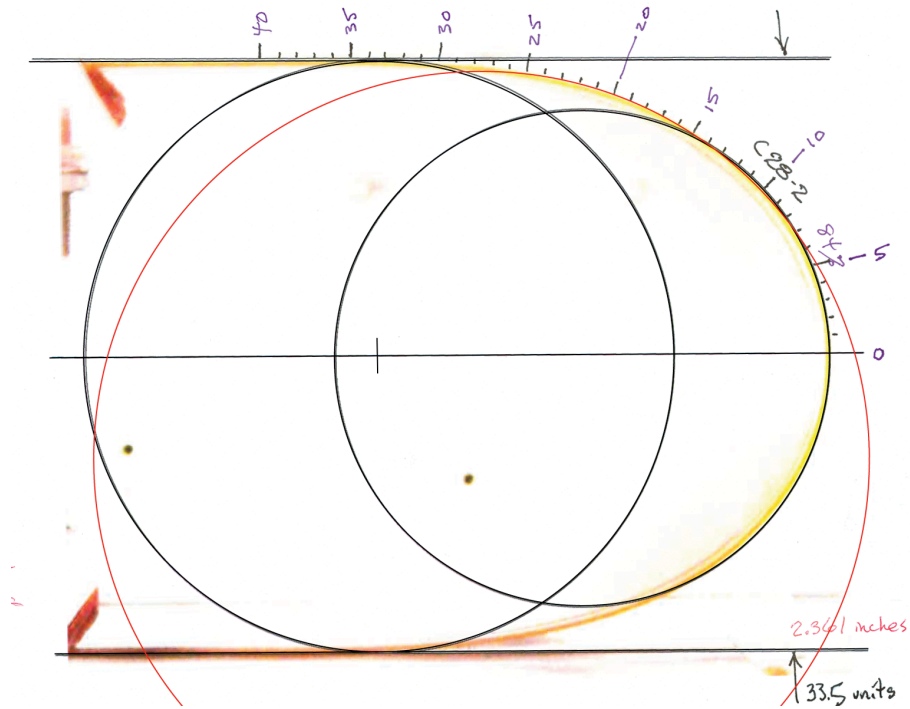


Figure 13. Sectional view of flex cable fold cross-section (see Figure 12).

The first approach taken was to try to find a functional form that would adequately describe the geometry of the fold. The closest approximation found was an ellipse. However, it had several problems that made it unsuitable. First, the radius of curvature at the tangent point to the constraining plate is finite. Second, an ellipse that fits the apex

and tangent point necks down too rapidly (curvature too small) behind the apex. While further work along this line is possible, it proved expedient to abandon this approach for present purposes.

The second approach taken was to visually fit circles to a photograph of a folded (straight) cable, as illustrated by the red circle in Figure 13. This proved to be practical only for the first 60% or so of the distance along the cable from the apex to the constraint tangent; as the radius of curvature grew too large, the uncertainty in the fit became unacceptable. However, analysis of the “60%” data suggested that an equation of the following form is appropriate (all dimensions are inches) for the curvature of the outer surface:

$$R = 0.3 \tan^2\left(\frac{\pi d}{2L}\right) + A$$

where

- R = radius of curvature (inches),
- d = distance along cable from fold apex (inches),
- L = distance along cable from apex to tangent point at constraint (inches), and
- A = radius of curvature at apex (inches).

To overcome the limitations associated with visually fitting circles to an image, a third approach was taken that digitized points along the outer edge of the cable using a Cartesian coordinate system (x-y pairs plus d, distance along cable from fold apex). Since the radius of curvature is given by:

$$R = \frac{\left[1 + \left(\frac{dy}{dx}\right)^2\right]^{3/2}}{\frac{d^2y}{dx^2}}$$

it was then possible to apply simple finite-difference algorithms to the points to develop a description of the behavior of R as a function of position relative to the apex. The drawback to this approach is that “noise” in the data (e.g., uncertainties in identifying the cable edge, measurement errors, and uncorrected distortion due to camera perspective) is significantly “magnified” both in the process of calculating derivatives and in raising them to a power (as in the equation above). Nevertheless, the results so obtained provide

a basic understanding of how the cable bends in the region of the fold. An approximate, normalized fit—intended to be conservative in regards to strain calculations over the regions of most interest—was developed to support strain analysis efforts. It is of the form:

$$\mathcal{R} = \frac{0.3}{D} \tan^2\left(\frac{\pi d^{1.25}}{2\mathcal{L}}\right) + \mathcal{A}$$

where

D = characteristic fold “diameter” equivalent to the constraint dimension given in Table 5 (note that for the inside edge, the values in this table have to be reduced by twice the cable thickness given in Table 2),

\mathcal{R} = normalized radius of curvature = R/D ,

d = normalized distance along cable from fold apex = d/D ,

\mathcal{L} = normalized distance along cable from fold apex to tangent point at constraint = $L/D \approx 1$, and

\mathcal{A} = normalized radius of curvature at apex = $A/D = \xi/2$ (ξ is the apex radius reduction factor discussed in the text above, whose average is 0.87).

The calculated radius of curvature based on digital data manipulation and the two approximations are plotted in Figure 14 for reference.

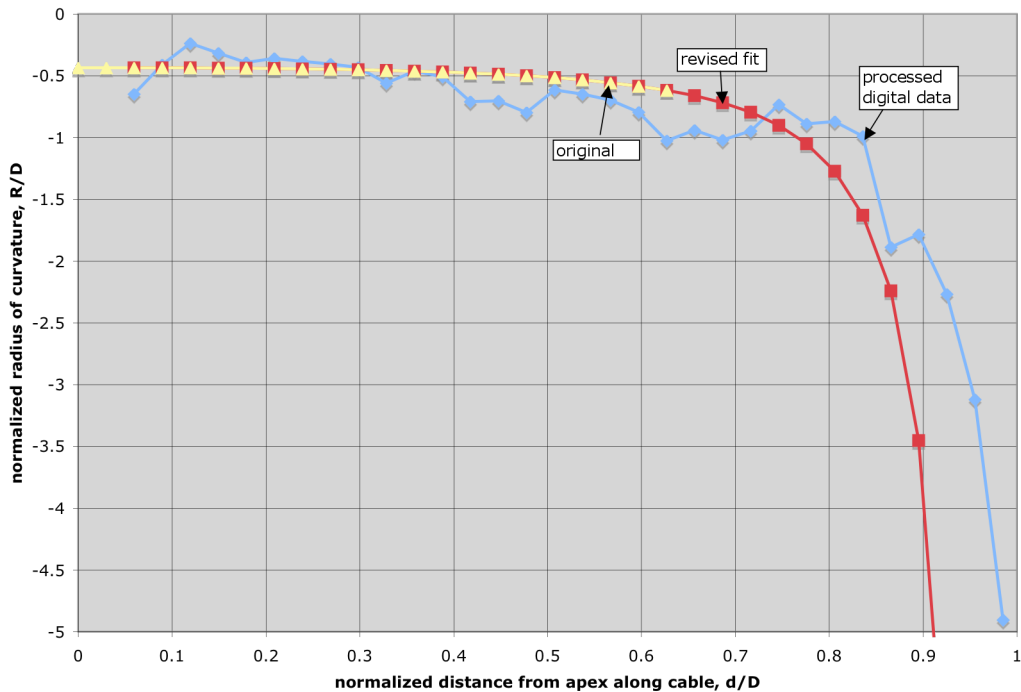


Figure 14. Flex cable fold radius of curvature behavior.

While further refinement would be possible with additional test specimens and fixturing (e.g., improved position digitalization tools), the results presented above are considered adequate for the purposes of this assessment. In terms of projecting these results onto a particular trace (e.g., trace edge) of concern, it is only necessary to replace ‘d’ in the equation for radius of curvature above with $\rho \sin \phi$, where ρ is the appropriate value for the radial location of the trace (from Table 3 and Table 4) and ϕ is the rotational angle from the apex fold line to the point being evaluated (and note that the distance from the fold line along the trace to the point is given by the product $\rho\phi$, with ϕ in radians).

A similar assessment can be made of the cable twist that is observed behind the fold in the cable. However, since twist-apex-to-plate and fold-apex-to-plate lengths are of the same order of magnitude¹¹ while the fold minimum radius of curvature is much smaller,¹² strains in the fold are bounding and will dominate fatigue behavior. However, where required to assess strain behavior, twist geometry will be modeled with an equation of the form:

$$y = ae^{-b(\theta-c)^2}$$

where the constants a, b, and c are determined based on an approximate fit to photographs such as those shown in Figure 10.

2.1.2 Number of Flexures

The C27 and C28 flat cables are required to flex repeatedly in support of telescope re-pointing events. The available field of regard (FOR; i.e., viewing angles) of the telescope spans the nominal pointing angle (“nadir”) $\pm 25^\circ$ in azimuth (C27) and $\pm 23^\circ$ in elevation (C28). In addition, relative to this nadir, when the telescope is stored or a radio calibration is performed, the azimuth is rotated -100° and the elevation is rotated -39° . However, while this range of motion has to be supported by the cables, requirements

¹¹ The peak in the twist appears at $\sim 110^\circ$ behind the fold line (relative to its unfolded position).

¹² Minimum twist radius of curvature observed was ~ 6 inches vs. ~ 1 inch for fold (c.f. Table 6); i.e., maximum strain in twist is $\sim 1/6$ th of the fold.

actually define object location and observation frequency, which can be directly translated into prototypic “day-in-the-life” gimbal rotational angles and timing data. These data, in turn, can be described by a cumulative distribution such as presented in Figure 15. If, based on this figure, 12° is considered to represent both the mode and median of “day-in-the-life” re-pointing angles, if the re-pointings are considered to cluster about the nadir, and if changes in elevation will typically be larger than those in azimuth in proportion to the different FOR angle requirements, then a little spherical geometry suggests that the mode for elevation re-points will be ~8 degrees while that for azimuth will be ~9 degrees. One day-in-the-life of the telescope will see ~320 such re-pointing events, or, over system life, ~1,160,000 re-pointings are expected (both of these values include a 2% margin to account for development testing and system checkout prior to use).

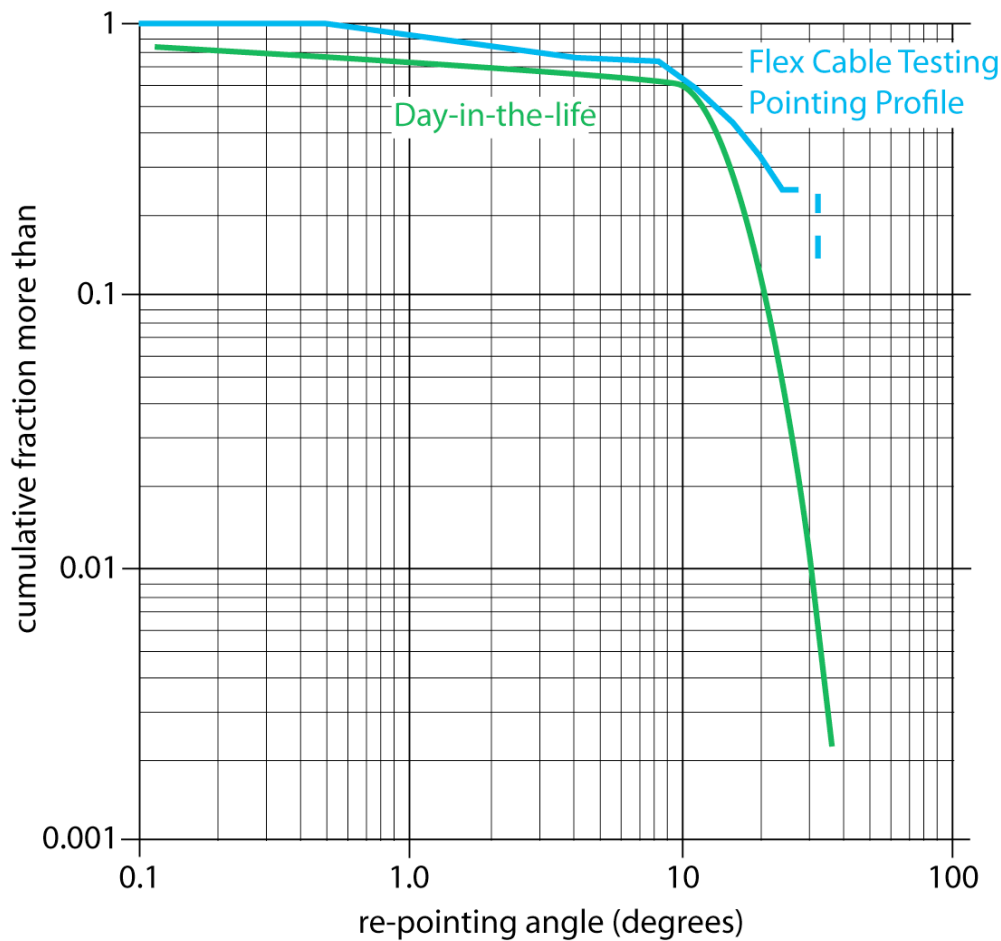


Figure 15. “Day-in-the-life” telescope gimbal re-points.

For cyclic fatigue, life depends on the applied strain range, which is the strain amplitude between the reversal points in the bending cycle. To compare the two (re-pointing events vs. bending cycle) some form of mapping is required. One approach is to assume that re-pointing events take place either beginning at nadir or on returning to nadir: one bending cycle then begins at nadir, a re-point involving a change in elevation and azimuth occurs, the system returns to nadir, another calibration re-point takes place with opposite signs in elevation and azimuth than the first, and then the cycle completes with a return to the nominal pointing direction. Thus in this simple fatigue damage model, four re-pointings make up one bending cycle; that is, one system life requires the flex cables to survive the equivalent of 290,000 bending cycles. However, one design requirement is to show the cables can survive twice system life, which would thus be equivalent to 580,000 cycles. That re-pointings pass through the “nadir” can be demonstrated by reviewing a plot of azimuth-elevation pointing data generated by day-in-the-life simulations, as in Figure 16, which supports this approach (in this figure, “nadir” is at a reference elevation angle of -20° while the azimuth angle is 0°).

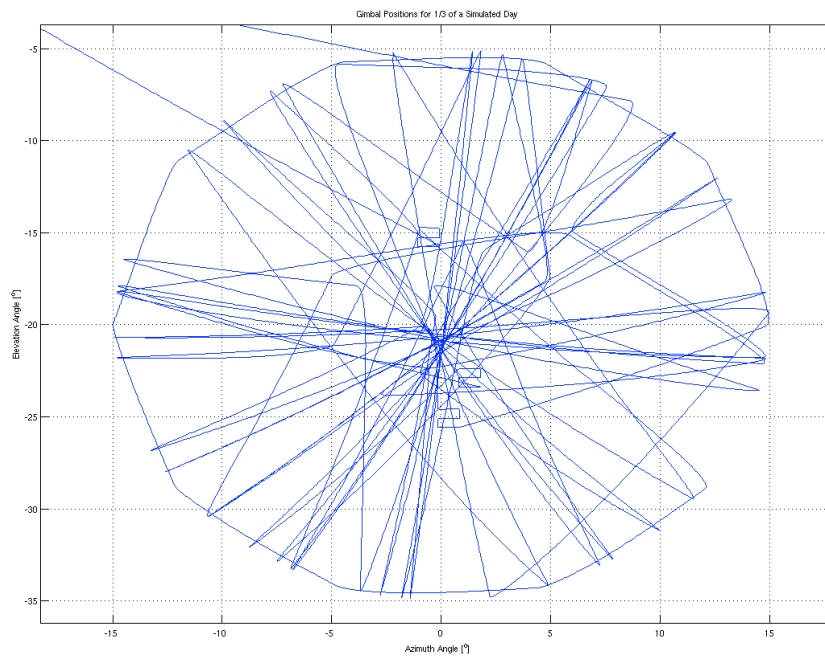


Figure 16. Gimbal positions for one-third of a day-in-the-life.¹³

¹³ Data provided by Curtis Webb, Sandia National Laboratories.

The availability of such a model suggests another way to map re-pointings to fatigue cycles: decompose the simulation data of Figure 16 into separate elevation and azimuth traces, as in Figure 17. Note that any angles developed from these data are conservative from a strain sense (an increased number of larger angles), as illustrated by the curve labeled “Flex Cable Testing Pointing Profile” in Figure 15.

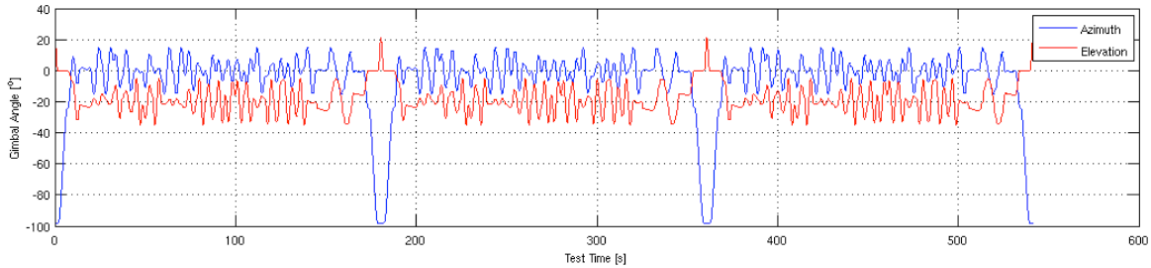


Figure 17. Gimbal positions for one simulated day-in-the-life.

By visually “filtering” out higher frequency components of the data presented in Figure 17, it appears that there are something on the order of 70 significant fatigue cycles per day (i.e., a design life requirement of ~260,000 cycles). In order to develop a manageable slew profile for the purposes of this paper, the data of Figure 17 were manually quantized into four different bins: $\pm 5^\circ$, $\pm 10^\circ$, $\pm 15^\circ$, and $+10^\circ/-39^\circ$ (for elevation) or -100° (for azimuth); the results are presented in Figure 18.

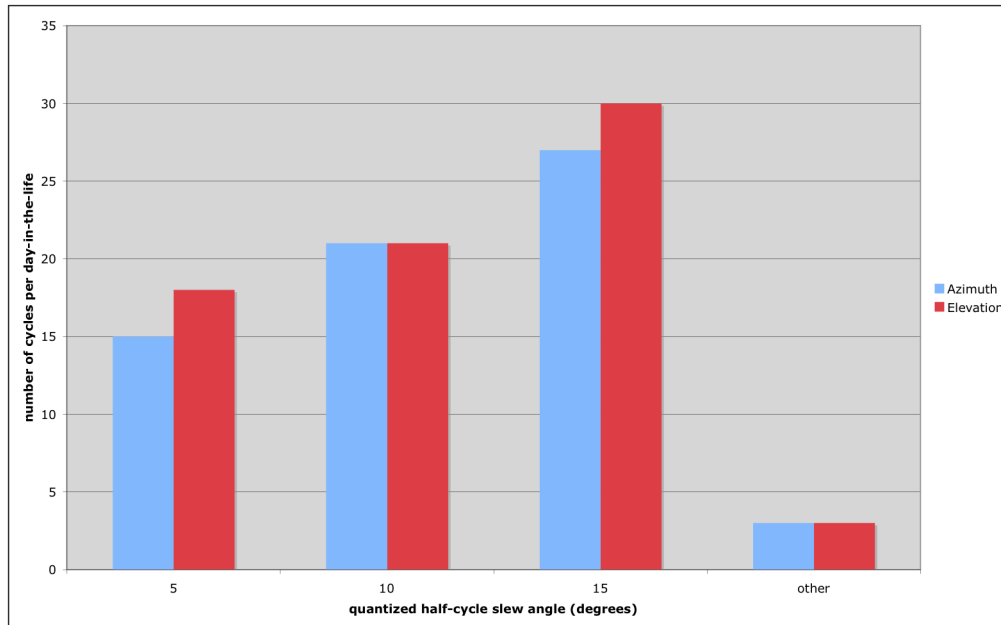


Figure 18. Simplified day-in-the-life elevation and azimuth pointing model.

Conceptually—with sufficient analytical investment—it should be possible to refine this bending cycle model as a function of position along the cable, and so support generation of an applied strain range distribution as a function of position; however, such a task was far beyond the scope of this case study.

2.1.3 Maximum strain-range calculations

For cyclic fatigue, the cumulative fatigue damage depends on the applied strain range, $\Delta\varepsilon_{\max}$, which is the strain amplitude between the reversal points in the bending cycle.

Thus,

$$\Delta\varepsilon_{\max} = \varepsilon_{+\text{Reversal}} - \varepsilon_{-\text{Reversal}}$$

where $\varepsilon_{+\text{Reversal}}$ and $\varepsilon_{-\text{Reversal}}$ have to be determined for the extreme reversal positions during a flex cycle.

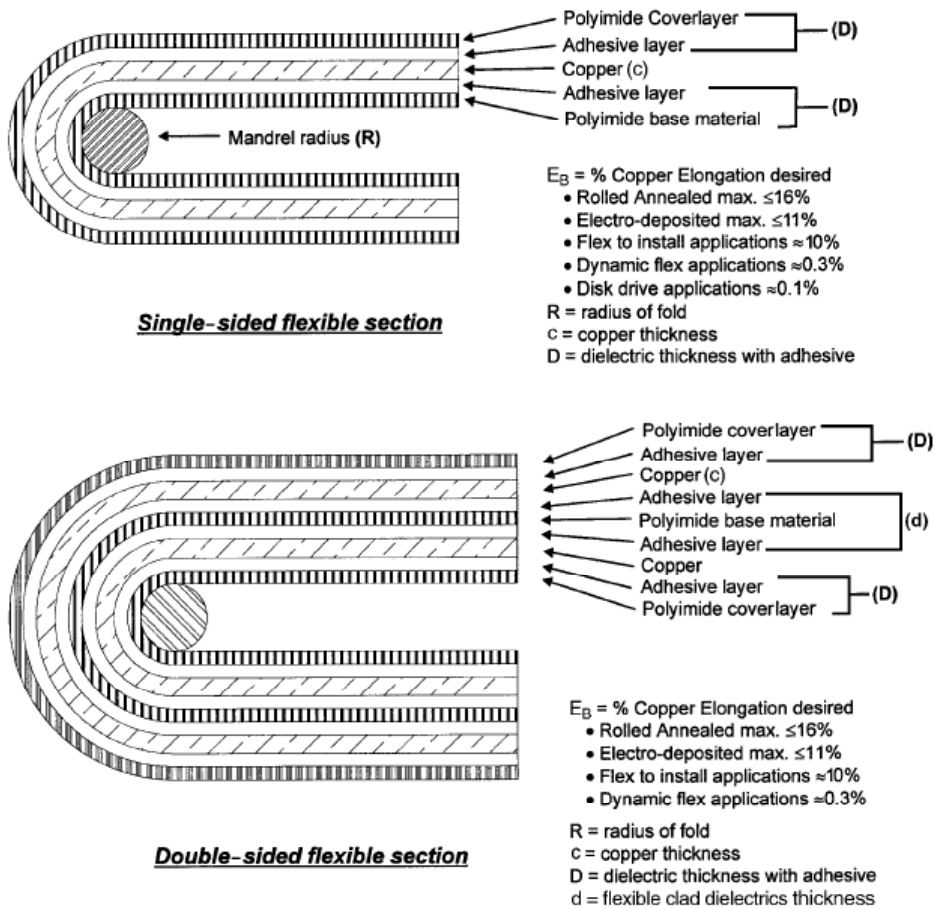


Figure 19. Nomenclature for layer stress analysis (from IPC-2223 Figure 5-7).

Following the bending model and nomenclature of Figure 19 (although replacing E with ϵ), the maximum strain for a single-sided flex cable of the design shown is given by:

$$\epsilon_{\max} = \epsilon_{t \max} = -\epsilon_{c \max} = \frac{100\left(\frac{c}{2}\right)}{\frac{c}{2} + D + R}$$

Similarly, for a double-sided flex cable—assuming that the conductor patterns are essentially identical—the maximum strain is given by:

$$\epsilon_{\max} = \epsilon_{t \max} = -\epsilon_{c \max} = \frac{100\left(\frac{d}{2} + c\right)}{\frac{d}{2} + c + D + R}$$

In these equations¹⁴ the ‘100’ converts the result to a percentage; otherwise the numerator represents the distance from the neutral bending (zero-strain) plane to the outer copper surface, while the denominator represents the distance (radius) from the center of the bend to the neutral axis.

For the double-sided cables C27-4 and C28-2, the conductor patterns are not identical, as presented in Figure 6 and Table 3 (i.e., the equivalent width of the signal traces is less than the ground plane), and so the relationship for the maximum strain in a double-sided flex cable given above needs to be corrected in some manner to account for this asymmetry. One approach is to use the concept of equivalent homogeneous cross-sections, the fact that the moduli of elasticity for the DuPont dielectric materials in the cable stack ups are ~2 orders of magnitude less than that of copper (and can so be ignored for purposes herein¹⁵), and the fact that moments of inertia about the neutral plane must be zero. This allows an approximation for the maximum strain in a cable to be developed based on the total conductor widths, w, for each side that is given by:

¹⁴ These equations are rearranged versions of those presented in IPC-2223 §5.2.3.4, and the equivalents of IPC-D-330 §7.11.1.

¹⁵ The different plastic behavior of these materials in tensile and compressive loading is also considered to be a secondary effect that is not considered here.

$$\epsilon_{\max} = \frac{100(\mu d + c)}{(1 - \mu)d + c + D + R}$$

where

$$\mu = \frac{W_{\text{ground plane}}}{W_{\text{ground plane}} + W_{\text{signal traces}}}$$

As suggested in §2.1.1 (p. 15 ff.), a first, conservative approximation of the strain range that the C27 and C28 cable sets will be experiencing can be made by assuming that it is equivalent in magnitude to the maximum strain found in the bend apex (i.e., the strain range is set by the maximum strain of the apex and the zero strain at the tangent point). Then, based on the data of §2.1.1 and the equations above, the results of Table 7 below can be calculated. The entries for C27-4 and C28-2 have been highlighted in Table 7 because the results exceed the 0.3% maximum for dynamic flex applications specified by IPC-2223 (see, e.g., the notes in Figure 19);¹⁶ all other entries have a 20% or more margin to this design limit.

Table 7. Maximum Strain Range Calculations¹⁷

Cable Layer	oz.	$\Delta\epsilon_{\max}$ l.l. (%)	$\Delta\epsilon_{\max}$ u.l. (%)
C28-2 (double CU)	1	0.55	0.73
C28-1 layer a	2	0.12	0.16
C28-1 layer b	2	0.12	0.16
C28-3 layer a	2	0.12	0.17
C28-3 layer b	2	0.12	0.17
C27-1 layer a	2	0.10	0.14
C27-1 layer b	2	0.10	0.14
C27-2 layer a	2	0.10	0.14
C27-2 layer b	2	0.11	0.14
C27-3 layer a	3	0.16	0.22
C27-3 layer b	3	0.16	0.22
C27-4 (double CU)	2	0.64	0.84
C27-5 layer a	3	0.17	0.24
C27-5 layer b	3	0.17	0.24
C27-5 layer c	3	0.18	0.24

¹⁶ In contrast, IPC-4562 Appendix A engineering data for this material that indicates the maximum strain range should be limited to 0.17% under *continuous* flexing conditions (without reference).

¹⁷ “l.l.” stands for lower limit and “u.l.” stands for upper limit as established by dimensional analysis.

2.1.4 Strain-range distributions

Further refinement of the strain-range results over those presented in Table 7 will proceed by selection of bounding or critical strain points at which the effects of the binned slew angles of Figure 2-18 can be considered. Clearly one critical strain point to consider is the fold apex. Another to consider would be the point where the cable is tangent to a physical constraint along the outside edge of the outermost trace. Finally, because the rotational angles are small (i.e., the maximum circumferential travel—other than for slews associated with the occasional stow or calibration—is less than the fold-apex-to-plate length), it is necessary to evaluate points that exhibit strain rates higher than those of the apex or tangent. The later can be identified by taking the derivative of the reciprocal of the radius of curvature model¹⁸ presented in Figure 14, as illustrated in Figure 20. This plot indicates that the peak strain rate is expected to occur at a normalized distance from the apex of ~ 0.84 .

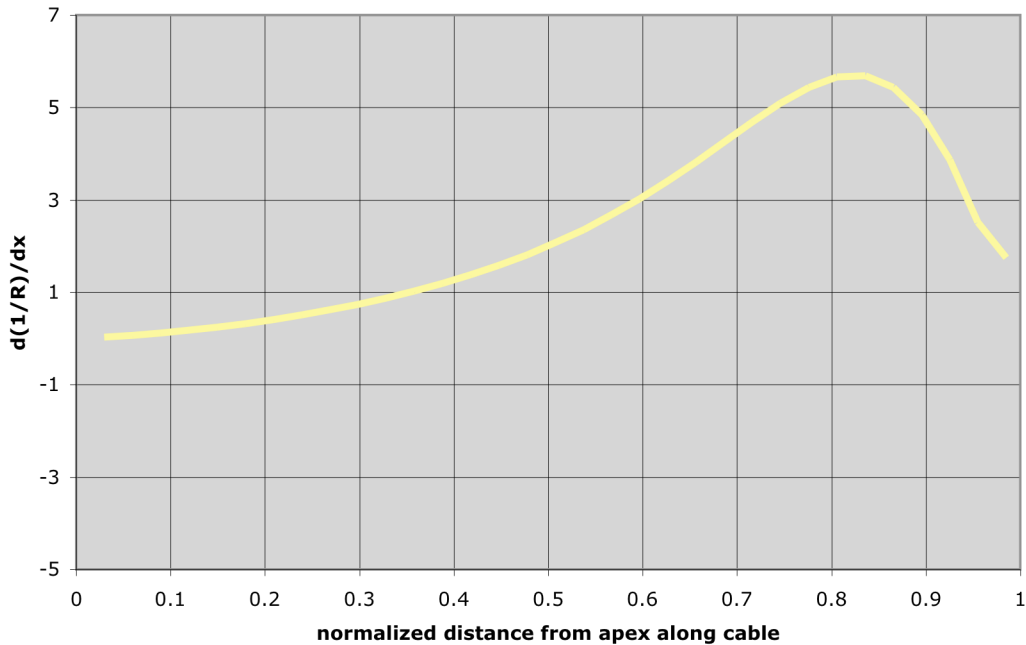


Figure 20. Strain-rate model.

¹⁸ Because the C27 and C28 flat cables are very thin compared to the radius of curvature, to a first approximation the strain is proportional to $1/R$.

The equations describing cable radius of curvature of §2.1.1 (including cable twist) and the relationships for strain given in §2.1.3 were combined into an engineering model of the strain along the omega sections of the C27 and C28 cables from the apex. An example profile is given in Figure 2-21; the peak strain is due to the cable fold, while the sinusoidal pattern in the tail of the curve represents the strain associated with the cable twist.

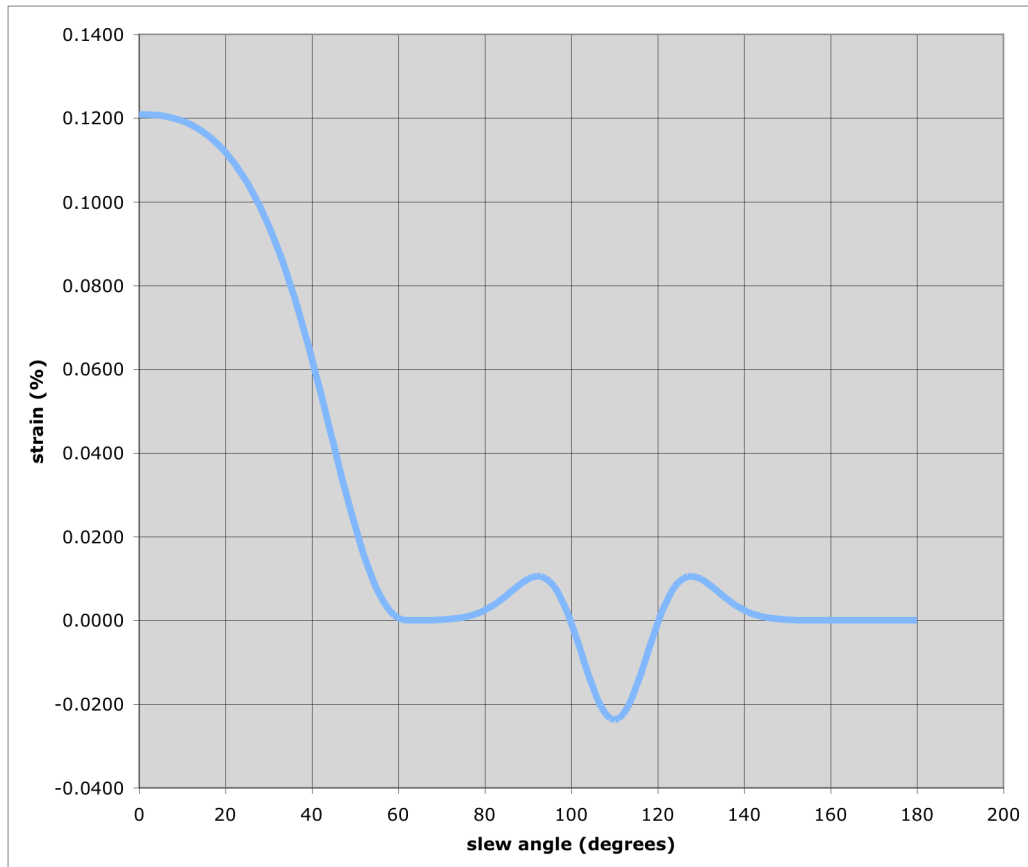


Figure 21. Example omega-flex cable strain profile for point originating at fold apex (C28-3 layer 2 outer trace edge shown).

This model was then applied to assess the strains in and maximum strain ranges experienced by each of the omega flex cable layers. Initially the apex, tangents, and maximum strain rate locations were evaluated for C28-3 layer 2 in order to identify the bounding (worse case) strain location—which turned out to be the maximum strain rate point that passes into the fold region during occasional re-pointing events associated with telescope stow or calibration. This is illustrated in Figure 22.

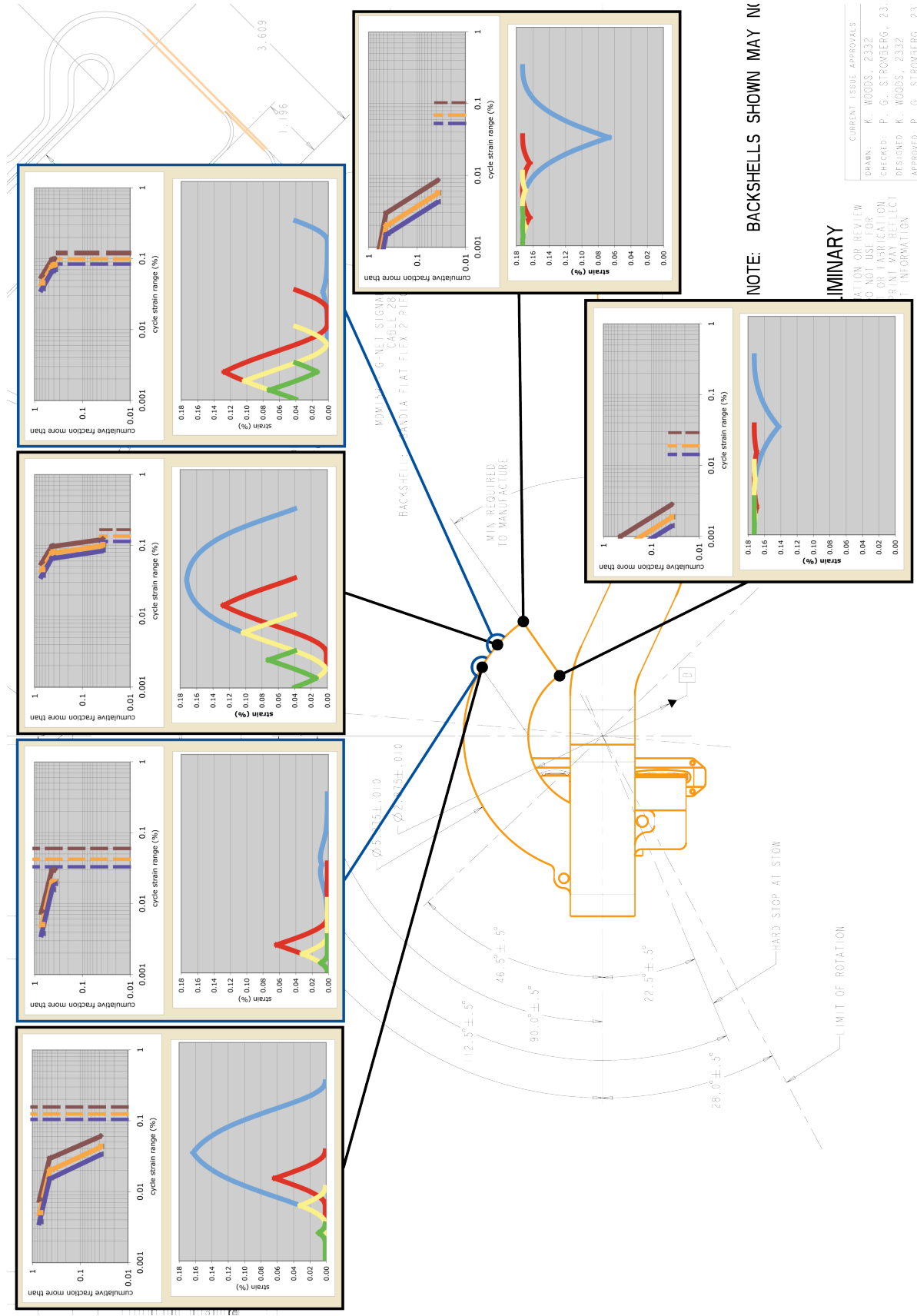


Figure 22. C28-3 layer 2 strains and strain-range distributions.

NOTE: BACKSHELLS SHOWN MAY NOT BE REPRESENTATIVE OF ALL BACKSHELLS

MINIMUM

FOR REVIEW
 NOT FOR FABRICATION
 PRINT MAY REFLECT INFORMATION

CURRENT ISSUE APPROVALS

DRAWN: K. WOODS - 2332
 CHECKED: P. G. STROMBERG, 2332
 DESIGNED: K. WOODS - 2332
 APPROVED: P. G. STROMBERG, 2332

The lower charts for each point analyzed in Figure 22 provide a plot of the maximum strain (worst-case mechanical tolerance stack up) for the point as it is rotated through the angles defined in Figure 18; here the green curves represent strain behavior for rotations of ± 5 degrees (i.e., from zero to +5 to zero to -5 to zero), the yellow for ± 10 degrees, the red for ± 15 degrees, and the blue for +10 to -39 degrees. The upper charts for each point represent a cumulative distribution for the minimum, nominal, and maximum strain ranges experienced by each point over a day-in-the-life (and life), with the total number of cycles defined as one quarter of the number of re-pointings (see the discussion in §2.1.2). Also shown are the strain and strain-range behaviors at the inner edge of the apex to illustrate, by comparison, that the maximums occur at the outer edge. Application of this approach to all of the cable layers yielded the maximum strain-range distributions shown in Figure 23.

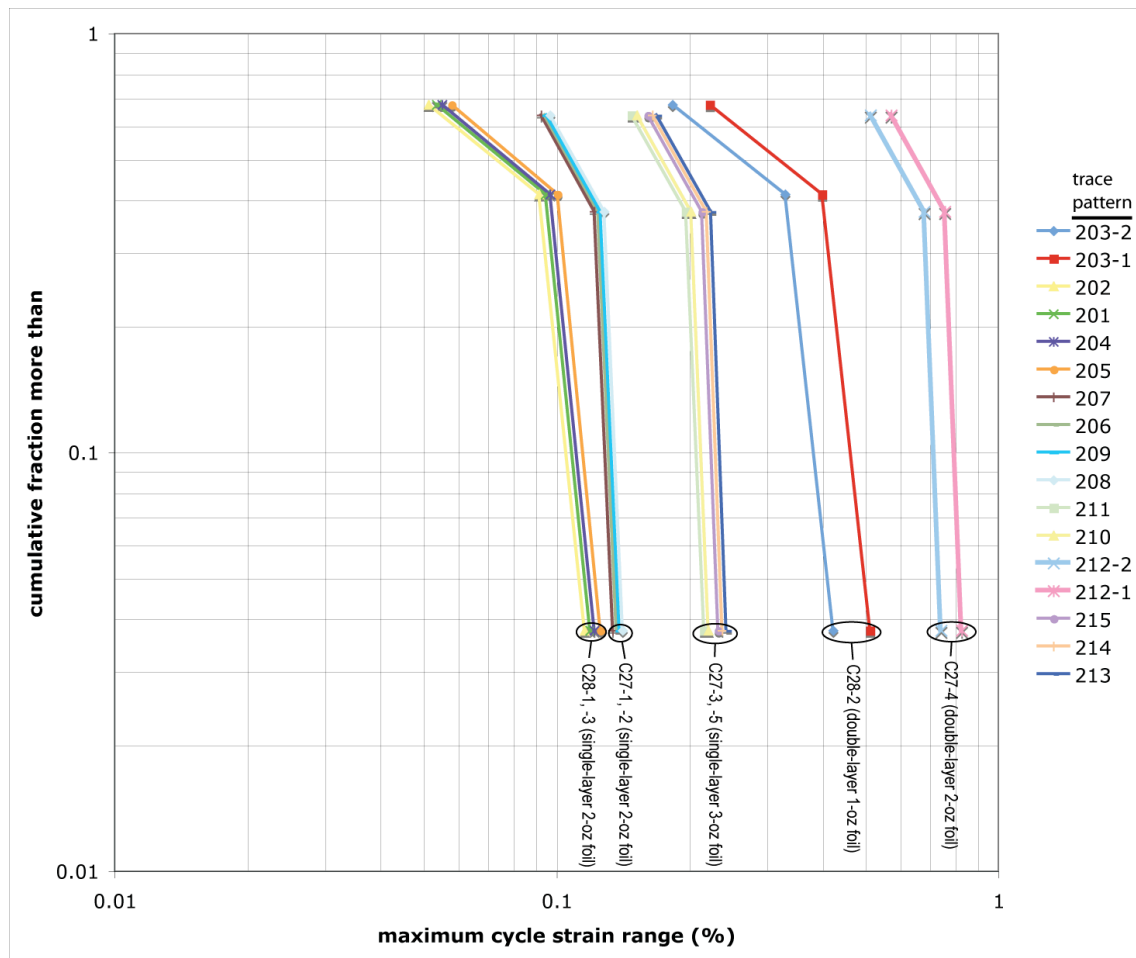


Figure 23. Maximum strain-range cumulative distributions for the omega flex cables.

Note on model validation: The strain behavior model presented produces results for the rotational angles of interest; the usefulness of the results is ultimately dependent upon the suitability (accuracy) of the radius of curvature model presented in Figure 14—and the derived strain and strain-rate models—in predicting the strain ranges found in the omega flex cables (e.g., Figure 22). Supporting evidence for the validity of this engineering model is available from the failures of prototype C27-4 cables mounted on a two-axis test bed, as shown in Figure 24 below. The photograph in this figure is an annotated montage created from a cable outline drawing, the artwork, and photographs from the failure reports. The yellow arrow in this image points to the location of the failure observed in S/N 002. Failures were also observed in this same area in S/N 003; additional failures in S/N 003 occurred within the area labeled “A”. Compare these failures to the annotations pointing out the bend apex at nadir (maximum strain) and to the predicted lines of maximum strain rate based on the model presented in this section. In other words, for the rotational angles and frequencies of interest, the model predicts worst case strain ranges occur along lines of maximum strain rates which lie away from the bend apex; and it is at or near such predicted maximum strain rate locations that actual failures occur.

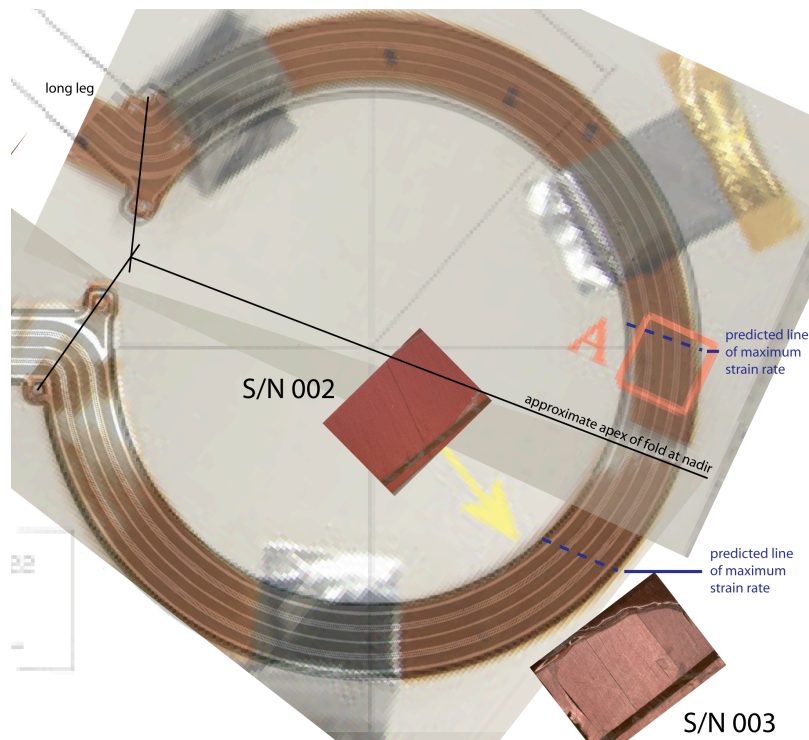


Figure 24. Prototypic test evidence in support of strain model.

2.2 Ductility Model

2.2.1 Materials selection

According to the cable vendor’s technical proposal and drawings, the omega flex cables are built with copper conductor material produced per IPC-4562 (or the preceding specifications IPC-MF-150 or IPC-CF-150). This is consistent with cables designed to IPC-2223. Foil designations under this specification take the form:

IPC-4562/X Where X is the specification sheet number	CU Foil Metal	E Foil Type	3 Foil Grade	2 Foil Thickness	S Bond Enhancement Treatment	XS Foil Profile	3 Quality Classification
---	------------------	----------------	-----------------	---------------------	---------------------------------------	--------------------	--------------------------------

The conductor materials specified to be used in the construction of the omega flex cables were electrodeposited copper (CU-E) designated as conforming to specification sheet 1 or 3 (or “slash” sheet from the form of the designator; i.e., IPC-4562/1 or IPC-4562/3), which corresponds to the foil grade designation (standard or high temperature elongation electrodeposited grade respectively). Foil thicknesses specified include 1-, 2-, and 3-oz in the original omega flex cable set design. Single-sided (S) bond enhancement treatment¹⁹ is specified, and is tied to the process used by the vendor in cable fabrication. Foil profiles are nominally specified in the material callouts as “LS” (low profile foil cathode side and standard profile foil anode/matte side, although note this is not consistent with the “S” bond enhancement specification), with “XS” (no treatment or roughness on the foil cathode side) identified as an acceptable alternative per drawing notes.²⁰ Figure 25

¹⁹ Bond enhancement involves deposition of an additional layer of copper in such a way that the resulting surfaces are rough (i.e., easier for dielectric material bonding to the surface), and are matte in appearance.

²⁰ Foil surfaces with “no treatment” are typically shiny (i.e., unless stored for a sufficiently long time and in an environment allowing surface oxidation to take place); for “XS” foil, it is likely that this side was adjacent to the titanium drum on which the copper was plated out onto. Also note that while the drawings ostensibly support use of “LS” foil (i.e., foil treated on both sides), there is no evidence of its actual use in the as-built omega cables, nor would it be consistent with current manufacturing processes (the “S” side is bonded to a substrate followed by a roughening of the remaining side by a manual process to enhance later bonding of the cover lay material).

provides several scanning electron microscope (SEM) photographs of a typical foil cross section, and of treated and untreated surfaces. Finally, while the product specification found in the drawings does not address quality classification, as all vendor material purchase orders have required chemical and physical analysis; this is equivalent to requiring high levels of assurance via the use of testing under quality classification 3.²¹

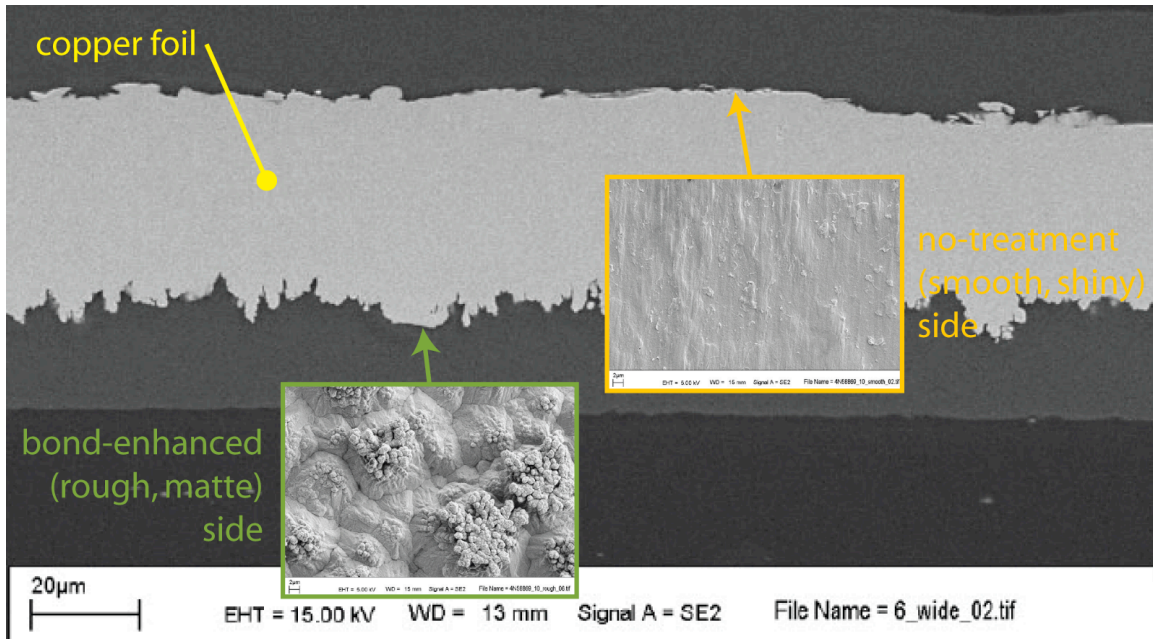


Figure 25. Representative SEM views of a copper foil cross section and surfaces.

The copper lot numbers for the actual materials used in constructing the original as-built telescope cable set are mapped by cable pattern number in Table 8.

²¹ Materials in class 3 are considered suitable for applications where high levels of assurance are required. “These levels of assurance **shall** be demonstrated via the use of testing and/or SPC/SQC techniques.” (IPC-4562 §1.3.)

Table 8. Copper Materials Selected for use in the Original Cable Build

Cable Layer	pattern no.	oz.	Copper Lot Number				
			28284 CU FOIL 1 oz CU-E(1)-1S-(LS-3) ³	58869 OAK-MITSUI 2 oz CU-E3-2S-XS3	59947 OAK-MITSUI 2oz CU-E3-2S-XS3	59915 OAK-MITSUI 2 oz CU-E3-2S-XS3	29091 CU FOIL 3 oz CU-E(1)-3S-(LS-3)
C28-1 layer 1	201	2		X			
C28-1 layer 2	202	2		X			
C28-2 "layer" 1	203-1	1	X				
C28-2 "layer" 2	203-2	1	X				
C28-3 layer 1	204	2		? ¹			
C28-3 layer 2	205	2		? ¹			
C27-1 layer 1	206	2			X		
C27-1 layer 2	207	2			X		
C27-2 layer 1	208	2		X			
C27-2 layer 2	209	2			X		
C27-3 layer 1	210	3					X
C27-3 layer 2	211	3					X
C27-4 "layer" 1	212-1	2		X			
C27-4 "layer" 2	212-2	2		X			
C27-5 layer 1	213	3					X
C27-5 layer 2	214	3					X
C27-5 layer 3	215	3					X
tensile strength (psi)			47400 ²	55120	54602	55440	47400
ductility tests conducted ⁴			X	X		X	X

NOTES: 1. As-built data not available at the time this document was drafted. However, as this cable was built under the same P.O. no., delivered under the same invoice no., and received on the same date as C28-1, it is likely that the same material lot was used in its manufacture.

2. Although lot tensile strength data was not provided as part of the material certification, based on available information it is reasonable to use the value of other CU FOIL products (e.g., lot 29091 data).

3. The use of parentheses in the foil designation in this table denotes information implied where otherwise not available from the available material certification records.

4. Ductility tests conducted at SNL following IPC-TM-650 Method 2.4.2.1 & ASTM E 796 using copper samples provided by the cable vendor, as presented elsewhere in this report.

2.2.2 Conductor Ductility

While copper foil ductility investigations are well represented in the published technical literature base, the vast majority of the published studies are focused on the behavior of very thin foils suitable for use, e.g., in printer mechanisms and disk drives.²² The most applicable ductility data were found in IPC-TR-484, as reproduced in Figure 26.

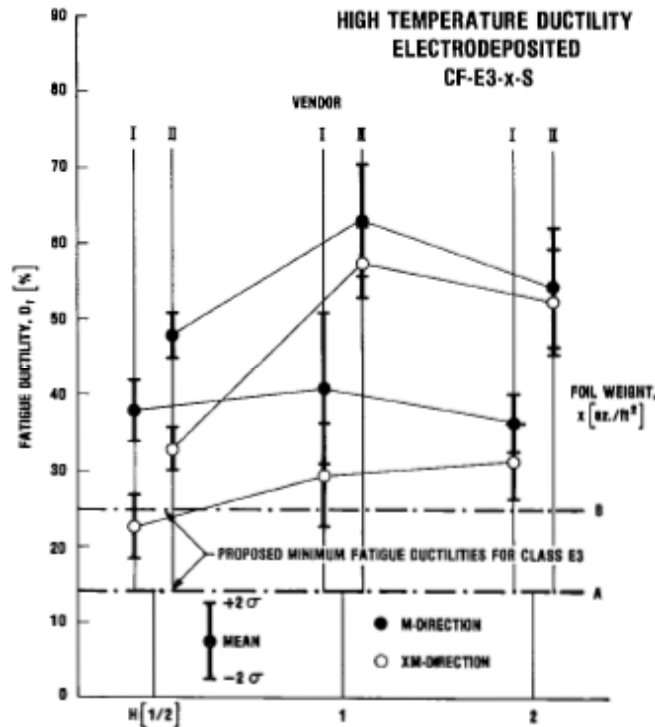


Figure 26. Ductility results for high temperature ductility electrodeposited copper foil, CF-E3, for various weights and foil vendors (IPC-TR-484 Figure 12).

While the data of Figure 26 could be of use in establishing design guidance, the preferred approach would be to test representative samples from the material actually used by the cable vendor. Such testing was carried out following IPC-TM-650 Method 2.4.2.1²³ and ASTM E 796 (see Figure 33 for a picture of the tester; note, however, that a cable test

²² See, for example, Merchant, H.D., M.G. Minor, and Y.L. Liu, "Mechanical Fatigue of Thin Copper Foil," *Journal of Electronic Materials*, Vol. 28, No. 9, 1999, pp.998-1007.

²³ Institute for Interconnecting and Packaging Electronic Circuits, "Flexural Fatigue and Ductility, Foil," *Test Methods Manual*, IPC-TM-650, Method 2.4.2.1, Lincolnwood, IL.

sample—not copper foil strip—is mounted in the unit).²⁴ Because of the stochastic nature of ductility measurements, and because it has been shown that copper foil ductility properties vary with orientation (as in Figure 26)—generally reported as machine (M) direction and cross-machine (XM) direction²⁵—multiple tests are required for each manufacturer’s lot in order to adequately characterize the material.

From a data analysis standpoint, the IPC method calls for reporting the average ductility based on at least three specimens, while the ASTM method calls for reporting the average and sample standard deviation. To provide better statistical measures, tests reported herein were generally based on ten samples. However, it has been shown that fatigue life data—including that of copper foil—do not exhibit normal or Gaussian distributions; rather, use of the Weibull distribution offers a more realistic method of addressing the statistical nature of fatigue data, and how it relates to the characterization of flex cable reliability.²⁶ Therefore, the copper foil fatigue data collected are presented in terms of a Weibull probability plot in Figure 27; as used here, N represents the number of cycles to failure for the particular test, while $Q(N)$ is the unreliability, which is a cumulative Weibull distribution based on the use of median ranks²⁷ for the data.

²⁴ American Society for Testing and Materials, “Standard Test Method for Ductility Testing of Metallic Foil,” ASTM E 796-94 (Reapproved 2000), West Conshohocken, PA.

²⁵ “Machine” refers to the orientation of the foil with respect to the rotating titanium drum on which it was plated; “M” would be perpendicular to the axis of rotation while “XM” would correspond to a direction that was parallel to this axis. Machine and cross-machine directional information was not available for the samples provided by the cable vendor. However, as the matte side of the foil was marked by numerous striae, it was possible to cut test samples that represented both the M and XM directions. Identification of which direction the samples mapped to assumed that the direction of the striae corresponded to the M direction.

²⁶ See, for example, Hayes, Charlie, “Characterization of Electrodeposited Copper for Dynamic Flex Applications (Part 2),” *INSIGHT*, March/April 2001, International Disk Drive Equipment and Materials Association, pp. 34-37, and Merchant, H.D., et al., “Fatigue Life Statistics for 18 μ m Foil Based Flexible Circuits,” FLEXCON ’98, September, 1998.

²⁷ Bernard’s approximation was used to approximate the median ranks.

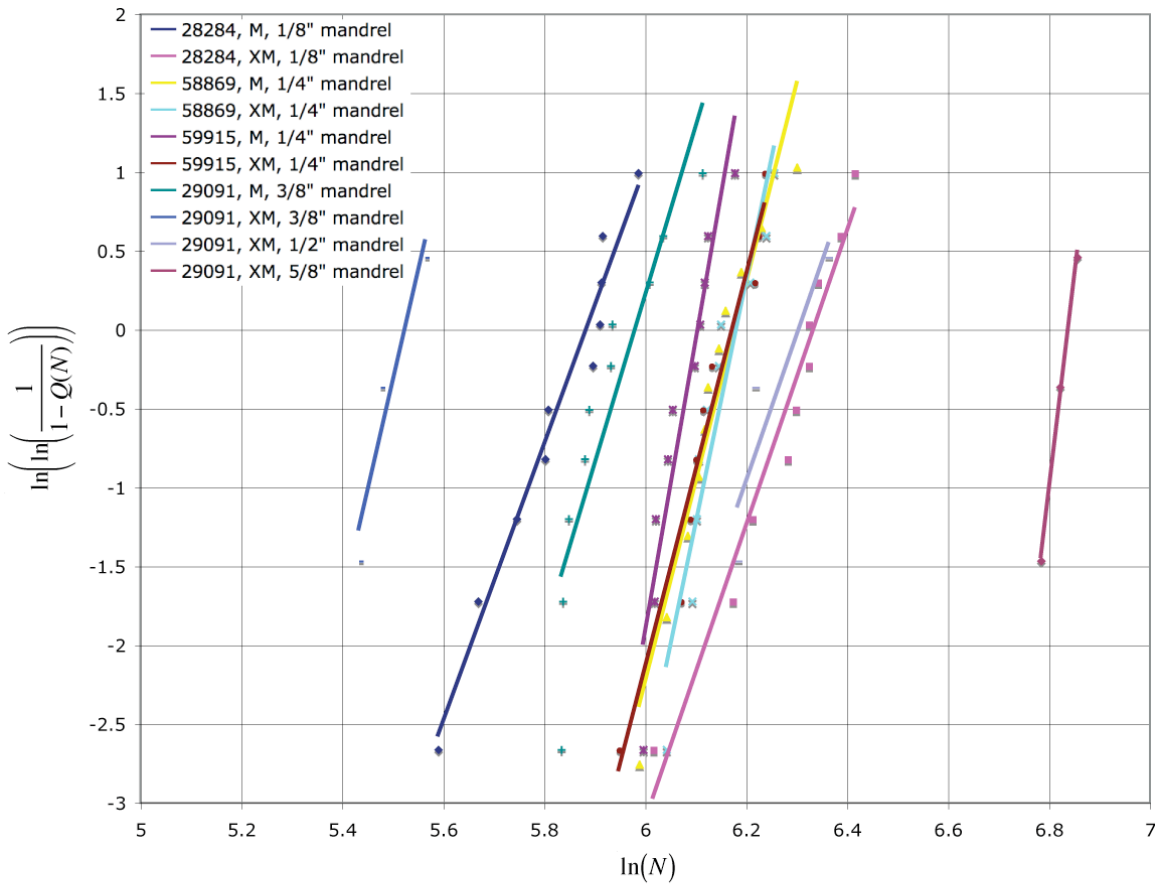


Figure 27. Weibull cumulative density plot of copper foil sample fatigue data.

Weibull parameters were developed by use of linear regression analysis—assuming the data followed a two-parameter distribution—that enabled, in turn, calculation of test run means and standard deviations. The Weibull slopes exhibited by the trends in the data, while seemingly high for general fatigue behavior, are characteristic of published foil ductility studies (e.g., Hayes, 2001, and Merchant et al., 1998). Four of the data sets (28284 M, 58869 M, 59915 M, and 29091 M) exhibit what appears to be a lower bound on cycles-to-failure, suggesting that use of a three-parameter Weibull distribution might be appropriate; however, as this behavior was not observed for all of the foil test series, without further testing the more conservative (for purposes herein), two-parameter distribution was selected for use.

Fatigue ductility values were then determined for each lot (refer to Table 8), following the iterative method set forth in the referenced standards, on the basis of the Weibull

statistical values. The results are presented in Figure 28 following the format of Figure 26 for comparison purposes. The vendor abbreviations in the figure refer to CU Foil (CU) and Oak-Mitsui (OM).

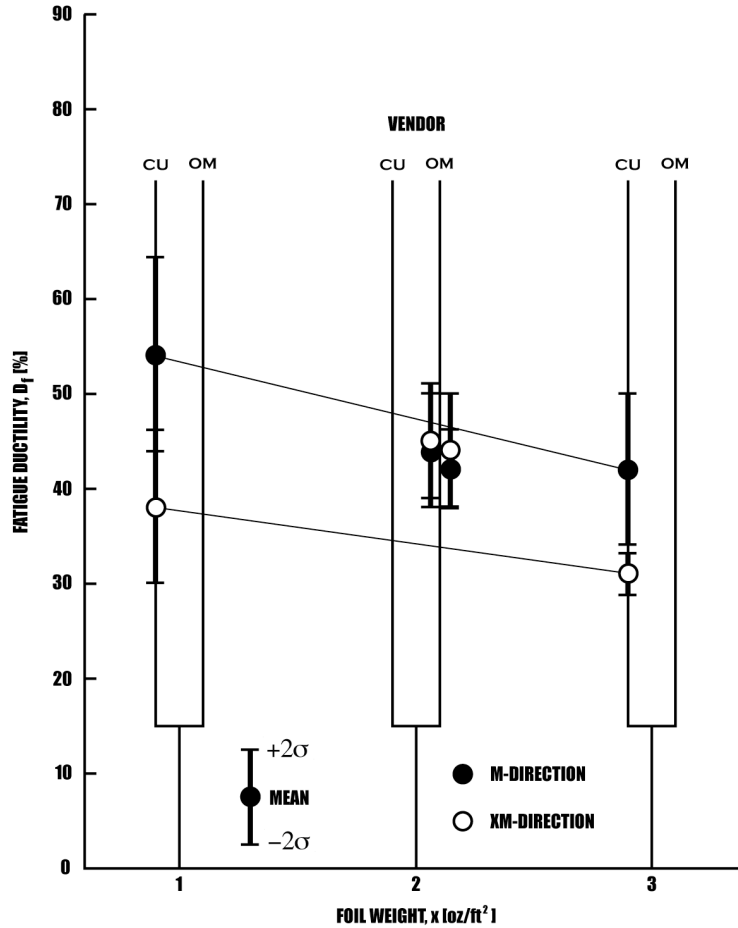


Figure 28. Ductility results for electrodeposited copper foil in use by the cable vendor.

Note that the apparent reversal in machine versus cross-machine direction ductility behavior exhibited by the Oak-Mitsui foil—as compared to the data for samples from the CU Foil and Figure 26 vendors—is not statistically meaningful. Further sample testing would be required to enable discrimination between the M and XM behaviors in Oak Mitsui foil.

2.2.3 Design Ductility

Foil ductility and tensile strength data can be used to provide a useful, generally conservative bound on cable fatigue behavior. However, there are a number of strong, second-order variables that can affect fatigue life. These include:

- The other materials in the composite cable structure (e.g., base laminate, adhesive(s), and overlay), which “can add two or three orders of magnitude to the flex life of the copper...[by] means of crack arrestment”²⁸ or strain relief.
- Manufacturing processes that may, intentionally or not, serve to anneal the copper foil, and so improve fatigue ductility performance.
- Manufacturing and handling processes which may, e.g., produce nicks, scratches, and pinholes, that effectively reduces the cross-sectional area of a circuit trace, and so reduce fatigue performance (usually characterized by an effective ductility reduction).

Examples of such effects from the published literature base are provided in Figure 29, Figure 30, and Figure 31 below. From an engineering standpoint, the individual effects of these variables are largely academic since they are reflected in product performance tests such as those conducted per IPC-TM-650 Methods 2.4.3²⁹ and 2.4.3.1³⁰ (provided they are conducted). However, awareness of such trends is useful to understand why shifts in performance (from bare copper foil to cable circuit) can occur, in support of possible product improvement efforts, and in setting product inspection or test requirements.

²⁸ Hayes, 2001.

²⁹ Institute for Interconnecting and Packaging Electronic Circuits, “Flexural Endurance, Flexible Printed Wiring Materials,” *Test Methods Manual*, IPC-TM-650, Method 2.4.3, Lincolnwood, IL.

³⁰ Institute for Interconnecting and Packaging Electronic Circuits, “Flexural Fatigue and Ductility, Flexible Printed Wiring,” *Test Methods Manual*, IPC-TM-650, Method 2.4.3.1, Lincolnwood, IL.

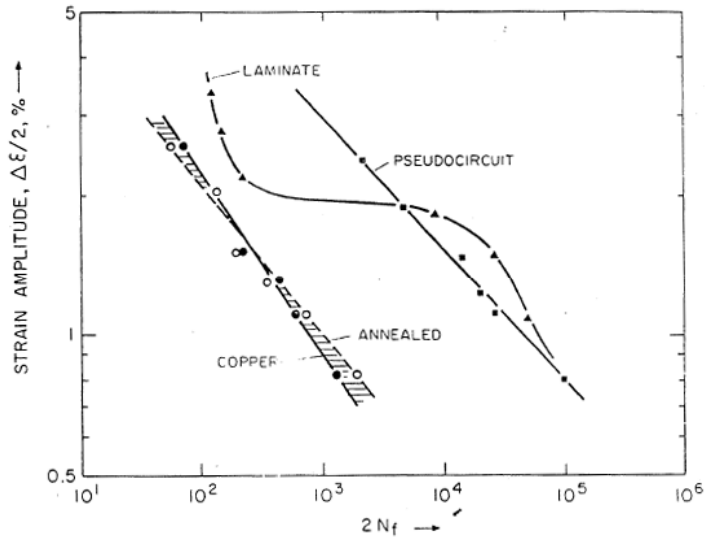


Figure 29. Coffin-Manson plot illustrating built-up cable (“pseudocircuit”) fatigue performance relative to bare copper foil.³¹

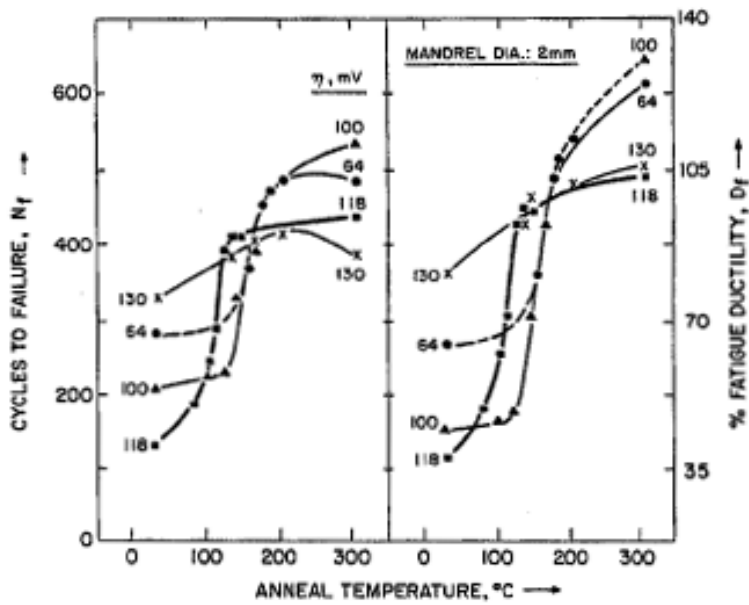


Figure 30. Copper foil fatigue data illustrating anneal temperature effects on ductility.³²

³¹ Merchant, H.D., S.K. Chiang, and M.G. Minor, “Flex Fatigue of Adhesiveless Copper Plateup on Polyimide,” FLEXCON ’96, Sunnyvale, CA, October 1996.

³² Merchant, Minor, and Liu, 1999.

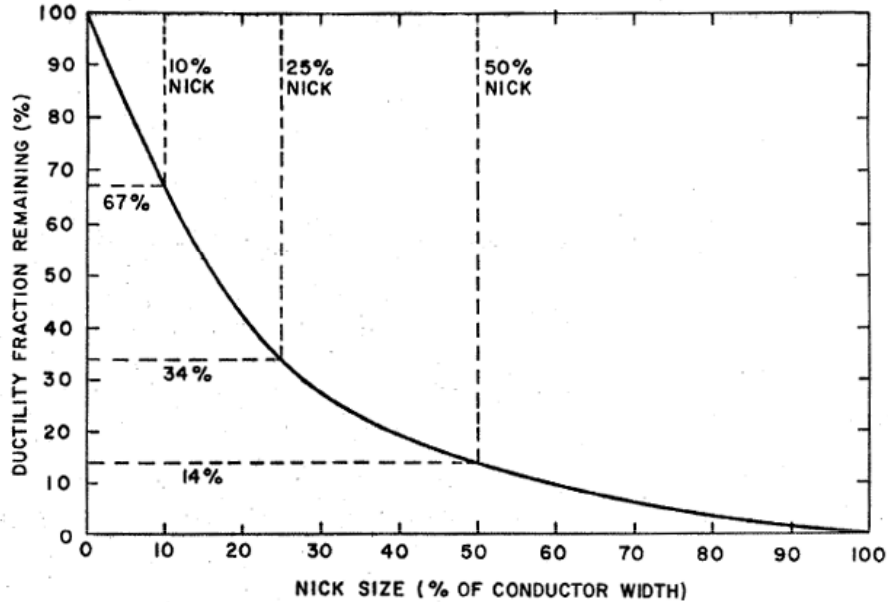


Figure 31. Reduction in available ductility due to conductor defects.³³

At one point the project had some concerns over the fact that the cable vendor deliberately scratched the “shiny” (non-treated) surface of the foil in a manual process using 3M “Scotch-Bright” pads, which conceptually could lead to a large loss in fatigue performance (as in Figure 31). Scratch depth measurements were subsequently taken³⁴ on a prototype C27-4 cable (S/N 003); the measured depths of 10 “large” scratches were (μm): 1.2, 1.2, 1.4, 1.8, 2.7, 2.8, 2.8, 2.9, 3.4, and 3.8. Based on the foil acceptance criteria of IPC-4562 §3.3.3, only the last of these scratches would “count” (the limit is no more than three scratches with a depth of $\geq 5\%$ of the nominal foil thickness per 300 mm x 300 mm area), and none would be sufficient for rejecting the material (scratches are not permitted where the depth is $>20\%$ of the nominal foil thickness). In other words, Figure 31 and the C27-4 cable scratch data might suggest that a 20% reduction in ductility over bare copper foil could be warranted due to defects introduced during the cable

³³ Engelmaier, Werner, “A New Ductility and Flexural Fatigue Test Method for Copper Foil and Flexible Printed Circuits,” 21st Annual IPC Meeting, Sheraton Park Hotel, Washington, D.C., April 1978. See also IPC-D-330 §7.11.3.2.

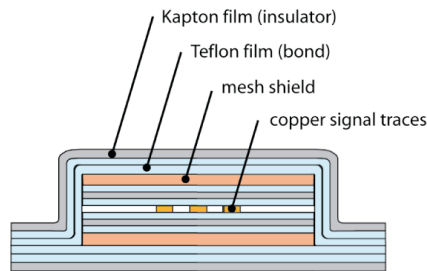
³⁴ Van Den Avyle, Jim, “SEM Cross-sections and Scratch Depth Measurements,” Sandia National Laboratories, Albuquerque, NM, 8/1/2006.

manufacturing process. However, that still begs the question of assessing the impacts of annealing and cable construction.

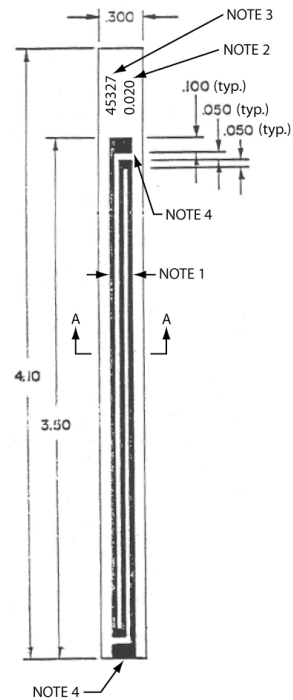
To assess the as-built cable performance, 2- and 3-oz standard copper test coupons³⁵ were constructed with prototypic cross sections and tested per IPC-TM-650 Test Method 2.4.3.1. The design of a typical test coupon is illustrated in Figure 32. Test samples were also constructed out of sections taken from prototype flex cables, which is allowable under test method §3.3 (as shown under test in Figure 33). In addition, a limited number of test specimens were evaluated in a manner considered equivalent to IPC-TM-650 Test Method 2.4.3 by the cable vendor (see Figure 34) that produced results of use here.

NOTES:

1. FOR TYPE-1 COUPON:
0.020 CONDUCTOR WIDTH,
0.020 SPACING,
0.100 PATTERN WIDTH (REF.);
ELSE, FOR TYPE-2 COUPON:
0.025 CONDUCTOR WIDTH,
0.025 SPACING,
0.125 PATTERN WIDTH (REF).
2. MARK WITH TRACE WIDTH.
3. MARK WITH 5-DIGIT LOT NUMBER
OF PRODUCTION LOT.
4. LAND FOR ATTACHING TEST LEAD
USING APPROPRIATE SOLDERING
METHODS. EACH LEAD IS TO BE OF
INSULATED, STRANDED WIRE OF
SUITABLE GAUGE, AND SHALL BE
10 +/- 2 INCHES IN LENGTH.
5. MATERIAL STACK UP TO
CORRESPOND TO LATEST
REVISION OF C27 AND C28
CABLE DESIGNS.
6. ALL DIMENSIONS SHOWN ARE
IN INCHES.
7. FIGURE NOT TO SCALE.



SECTION A-A (NOTE 5)



COPPER FOIL CIRCUIT TRACE PATTERN

IPC-TM-650 METHOD 2.4.3.1
TEST COUPON CONFIGURATION
SNL TYPE-1 AND TYPE-2
(ALTERNATE CONDUCTOR WIDTHS)

Figure 32. Typical test coupon used to develop flex cable fatigue design envelope.

³⁵ At the time of writing this report, the project had made the decision to replace use of 1-oz copper foil with 2-oz foil for improved current carrying capacity. Thus there was no need to develop a 1-oz design curve.



Figure 33. IPC-TM-650 Method 2.4.3.1 tester with installed cable sample.

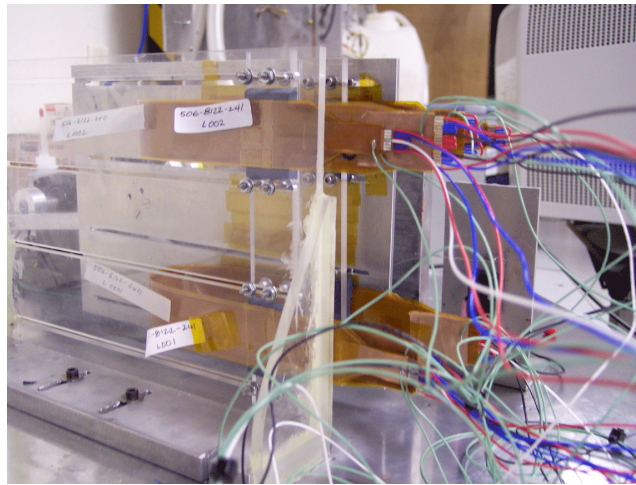


Figure 34. Vendor fixture used for conducting cable endurance testing.

By intent, test coupons are fabricated with traces of a single width. Ideally, a statistically significant number of tests would be conducted for each conductor trace width, thickness, and material vendor/type/lot combination intended for use across the flex cable sets. However, if the different width-thickness combinations—as presented in Table 3—are considered alone, a complete test matrix would require hundreds (if not thousands) of tests. A minimal test matrix can be developed, however, by making use of the fact that narrow trace widths exhibit reduced flex lives relative to wider traces (due to consideration of flaw-size-to-conductor-width ratios, crack propagation times, and strain

relief possibilities³⁶), and so testing can be limited to the narrowest trace width for each foil weight used in the design; the resulting design curves would be bounding for all other trace width-foil weight combinations.

The results for the various types of test specimens (discussed above) available at the time of writing are presented in Figure 35. The strain-range values plotted for the test results correspond to calculations based on nominal material thicknesses and test fixture dimensions. For reference, the six 3-oz data points lying at ~2% strain range (0.375-inch diameter mandrel) exhibit a Weibull slope of ~2.3; this is a typical value for fatigue failure (contrast the bare copper foil results of §2.2.2).

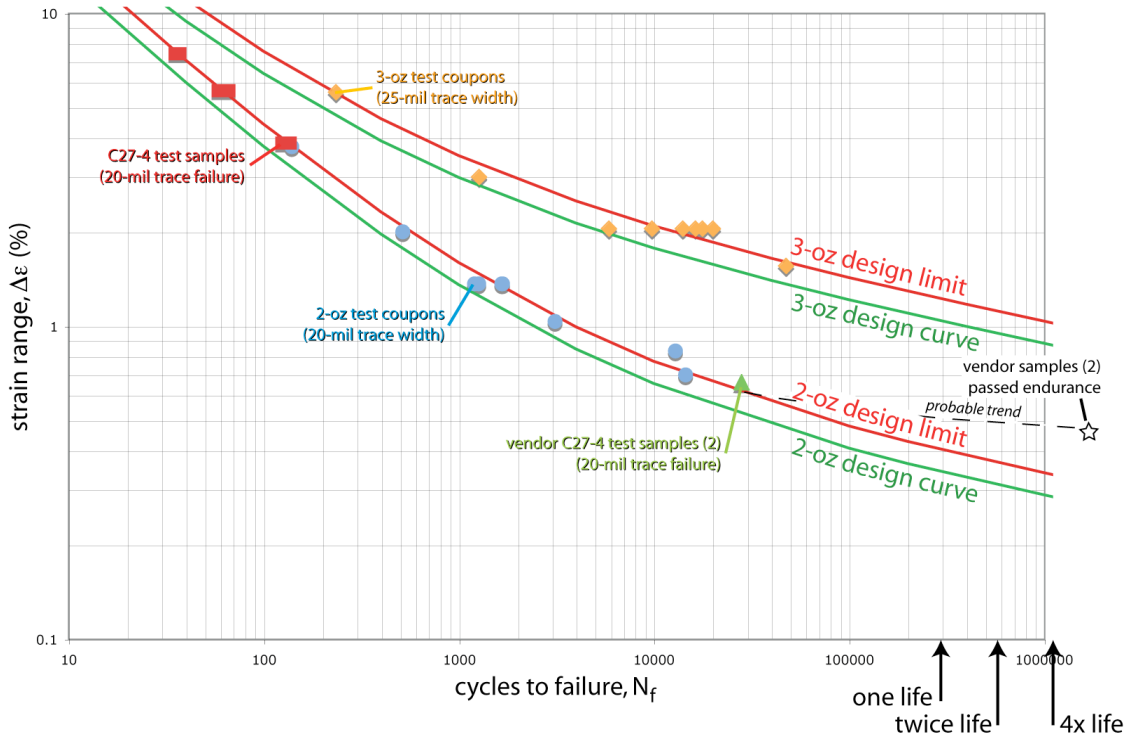


Figure 35. Omega flex cable design ductility model.

The relationships between fatigue life and strain range shown in the figure are modeled on the basis of the Manson-Coffin fatigue theory, which can be expressed in this application by the following empirical equation (IPC-TR-484 Equation 1 and IPC-D-330 Equation 7-16 corrected):

³⁶ As discussed in IPC-TM-650 Method 2.4.3.1 §3.2.

$$\Delta\varepsilon = N_f^{-0.6} D_f^{0.75} + 0.9 \frac{S_u}{E} \left[\frac{e^{D_f}}{0.36} \right]^{0.178 \log \frac{10^5}{N_f}}$$

where

- $\Delta\varepsilon$ = fractional strain range,
- N_f = fatigue life, cycles-to-failure,
- D_f = fractional fatigue ductility,
- S_u = ultimate tensile strength,
- E = modulus of elasticity.

The ordinary “least-squares” method was used to fit this model to the available fatigue-failure data for the two different foil weights used, and which are referred to as a *design limit* in the figure. Note that very limited data exist (“vendor samples (2) passed endurance”) suggesting that the resultant fits are conservative for high-cycle life.

Each design limit is matched by a *design curve* representing a 15% reduction in the allowable strain range for any given N_f . This 15% provides a margin of safety that is equivalent to the recommendations of MSFC-HDBK-505 701(3a),^{37,38} all cable designs should fall below the appropriate design curve. “One life” in the figure corresponds to design requirements in terms of the “detailed design life cycle history”—set forth in §2.1.2—as required by MSFC-HDBK-505 701(1). “Twice life” is shown for reference because of a requirement to provide verification data indicating the design will support twice design life.³⁹ “4x life” is also indicated because of the MSFC-HDBK-505 701(3b) requirement that the “fatigue analysis shall demonstrate a minimum calculated life of 4.0 times the required service life.”

While the results shown in Figure 35 provide the desired design guidance, they are somewhat surprising. Based on the published literature base, it was expected that the

³⁷ Bianca, Carmelo, *Structural Strength Program Requirements*, MSFC-HDBK-505, Rev. A, George C. Marshall Space Flight Center, Huntsville, AL, January 1981.

³⁸ The requirements of MSFC-HDBK-505, Chapter 7, “Fatigue”, are to be applied, as appropriate, to the flex cable life analysis per a derived project requirement.

³⁹ This was another derived project requirement.

built-up cable structure would exhibit fatigue lives “two or three orders of magnitude”²⁷ higher than the bare copper foil data of §2.2.2. This was, in fact, observed for the 3-oz foil; however, the 2-oz data shows little or no change between the bare foil and built-up cable configurations.⁴⁰ The behavior is summarized in Table 9, where the parameters listed appear in the Manson-Coffin fatigue model equation presented above. Follow-on programs may benefit from further investigation (e.g., simple design changes may provide increased design margin and so improve cable reliability); note that the variables are: vendor, copper foil thickness, and copper conductor trace width.

Table 9. Omega Flex Cable Design Limit Fit Summary

	bare foil ¹		cable	
	average D _f (%)	Su/E	effective D _f (%)	effective Su/E
2-oz foil	~44	0.0046	45	0.0047
3-oz foil	~37	0.0040	60	0.015
NOTES: 1. See Table 8 and Figure 28.				

Note on model validation: For vendor cables constructed per §2.1.1, using either 2-oz or 3-oz copper conductors supplied by material vendors as set forth in Table 8, the ductility models presented above provide: (1) design curves, whereby if cables operate in the region below the applicable curve survival is to be expected; and (2), design limits that can be used to predict fatigue life for cables subjected to strain ranges greater than ~0.5% (2 oz) or ~1% (3 oz). Both applications require use of a suitable strain-range model, such as presented in §2.1.4. For case (1), information regarding reliability for some given confidence level is not available without further testing (which, in fact, would be described by an entire suite of curves lying below the design limit); reliance must be placed on the suitability of margins established by other specification (such as that specified by MSFC-HDBK-505 as given here). For use case (2), supporting evidence for the validity of applying this engineering model to flex cables is available from the failure of prototype C27-4 S/N 003 cable on the two-axis test bed, as summarized below.

⁴⁰ For further discussion on these observations, see Beck, David F., et al., “Fatigue Behavior of Thin Cu Foils and Cu/Kapton Flexible Circuits,” *Materials Science and Technology (MS&T) 2008*, Pittsburgh, PA, October 6, 2008.

The strain-range model of §2.1.4 was applied to the prototype C27-4 cable design in order to develop a “load” spectrum using *nominal* dimensions, as the intent is to predict failure and not prevent the same (cf. the *maximum* strain-range behavior in Figure 23). This load spectrum is shown on the left side of Figure 36 on a cycles-per-year basis (solely for the purposes of presenting the result on the same plot as the design limit). The upper four data points in this spectrum correspond to the slew-angle model presented in Figure 18. The fifth, lower point represents the residual (small) re-points otherwise excluded in the slew-angle model in order to illustrate they are not important in a fatigue damage sense (see below); for this analysis, these small re-points were assumed to result in a strain-range equivalent to that imparted by slew angles of ± 2 degrees (conservative from a design standpoint).

The prototype C27-4 load spectrum was then combined with the 2-oz *design limit* (again, the intent is to be predictive) using a linear damage model (Miner’s approach^{41,42}). The resulting damage spectrum is shown to the right of Figure 36. Note that the residual re-points in this model are only responsible for $\sim 0.3\%$ of the damage, and so can safely be ignored (along with concerns over the impact of system jitter) for the present application.

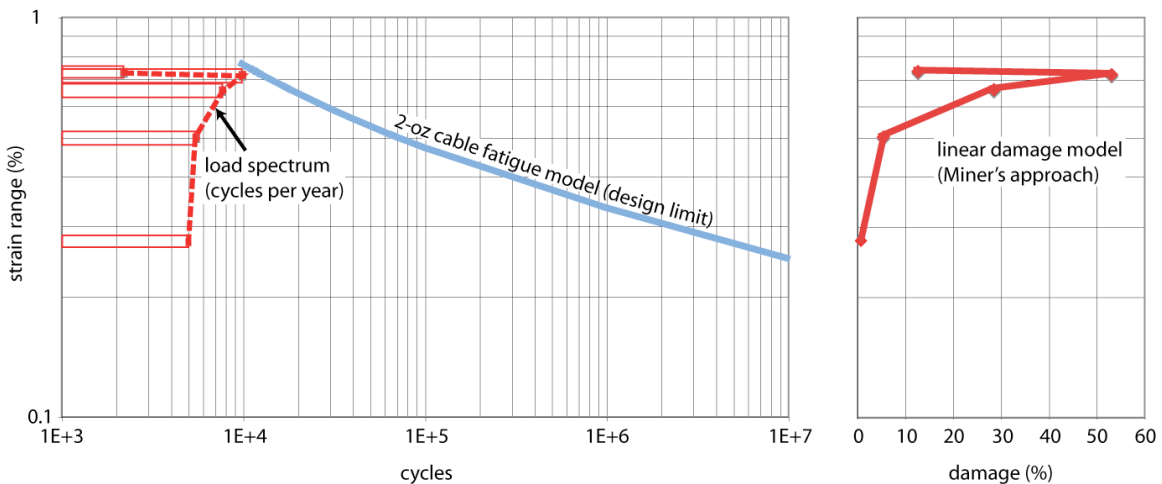


Figure 36. Prototype C27-4 cable fatigue damage model.

⁴¹ Miner, M.A., “Cumulative damage in fatigue,” *Trans. ASME*, Vol. 67, A159, 1945.

⁴² Consistent with derived project requirements and MSFC-HDBK-505 701(2).

The final result of applying this linear damage model to the prototype C27-4 cable is that an operational life of 240 days would be predicted. The prototype C27-4 cable actually failed in the two-axis test bed at ~160 simulated days. Since Miner's method is only expected to give order-of-magnitude results,⁴³ these predicted and observed values can be considered to be in agreement. Furthermore, Miner's method is known⁴⁴ to over estimate fatigue life in random loading conditions (as here), which provides further support to the agreement between these results.

2.3 Design-life Assessment

2.3.1 Cable strain-range spectra

The strain-range model of §2.1.4 was applied to the prototype flex cable set designs in order to develop a *maximum* "load" spectrum (e.g., worst-case dimensions) following the slew-angle model presented in Figure 18. This data was previously presented as a cumulative, per cycle distribution in Figure 23. The results are presented in Figure 37 (2 oz) and Figure 38 (3 oz) below in terms of 4x-life spectra following the MSFC-HDBK-505 701(3b) requirement.

⁴³ See, for example, Osgood, Carl C., *Fatigue Design*, 2nd ed., Pergamon Press Ltd., Oxford, England, 1982, p. 47.

⁴⁴ See, for example, Madayag, A.F., *Metal Fatigue: Theory and Design*, John Wiley & Sons, Inc., New York, 1969, p. 131.

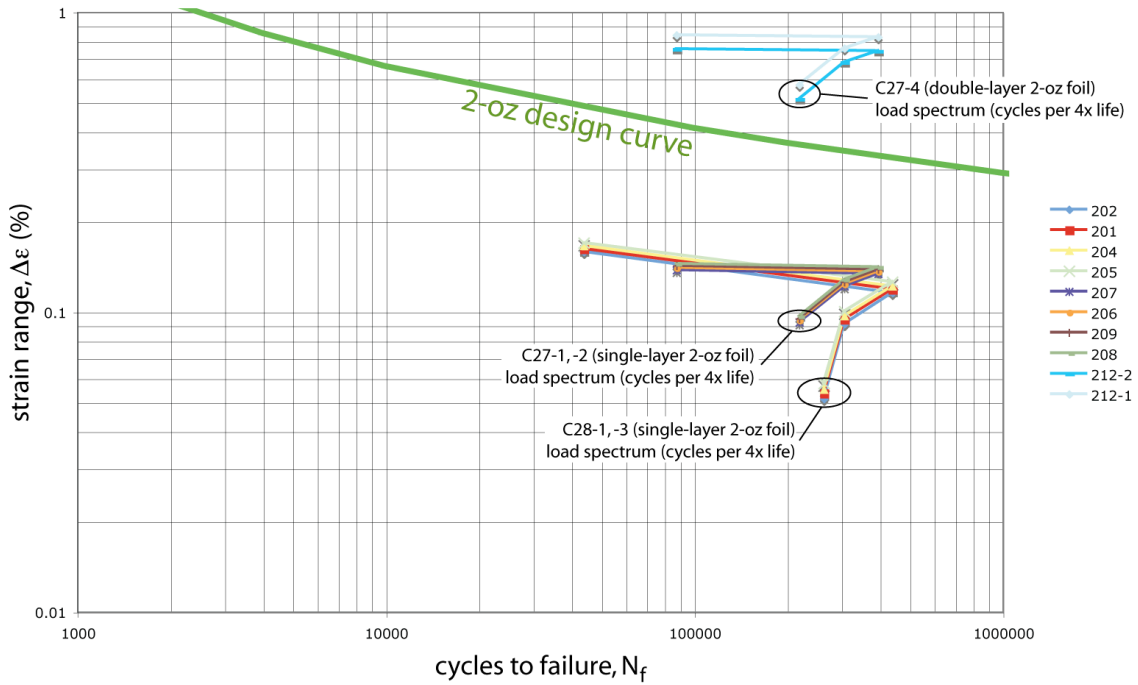


Figure 37. Strain-range spectra for the original 2-oz flex cables.

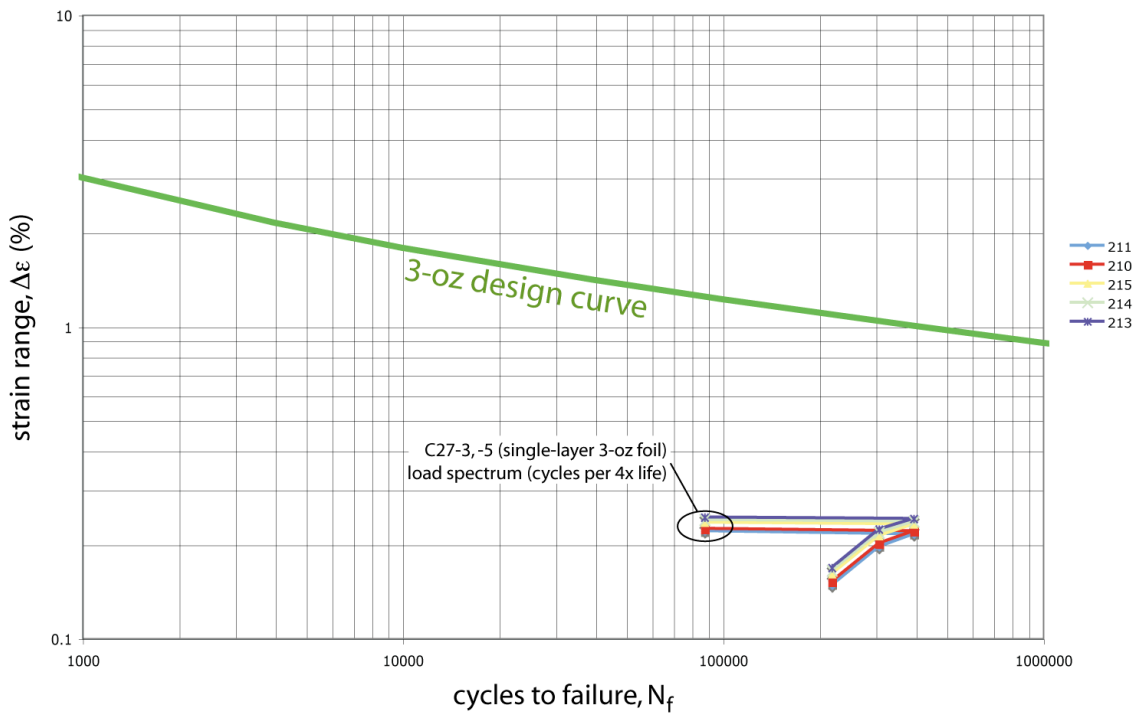


Figure 38. Strain-range spectra for the original 3-oz flex cables.

2.3.2 Flexibility Assessment

Interpretation of Figure 37 and Figure 38 is straightforward. The original C27-4 cable is clearly not acceptable in terms of life when compared to the 2-oz design curve. Even if the load spectrum for C27-4 was reduced by a factor of four (to one life), it would still exceed both the design curve and design limit. This is no surprise based on the observed C27-4 failures (see model validation discussions found in §2.1.4 and §2.2.3). It was also foretold by the simple assessment appearing at the end of §2.1.3.

2.4 Design Change Options to Achieve Desired Life

Three design changes are presented in the subsections that follow below, any one of which, if implemented, would allow the resultant omega flex cable sets to meet specified design lifetime requirements. For reference, the first option—replace double-layer designs with single-layers—was selected by the project, along with changing C28-2 to use 2-oz copper foil.³⁴

2.4.1 Alternate Configuration

The first choice for a revised omega flex cable set design would be to change the double-sided cables to a single-sided flexible printed circuits consistent with the “prudent design rules” of IPC-D-330 §7.11.4. Following the approach of §2.3 above, the load spectra for the “new” cable sets are provided in Figure 39 and Figure 40. From these it can be seen that all of the cables have a comfortable margin not only to the design limit, but to the design curve as well. The margin of safety (MS)⁴⁵ given for the curves was calculated as:

$$MS = \frac{1}{R} - 1$$

where

$$R = \frac{\textit{applied}}{\textit{allowed}}.$$

In this case, *applied* refers to the strain range a design is expected to see, while *allowed* refers to the appropriate design limit.

⁴⁵ This formulation for margin is called for by a derived project specification, which requires $MS \geq 0$.

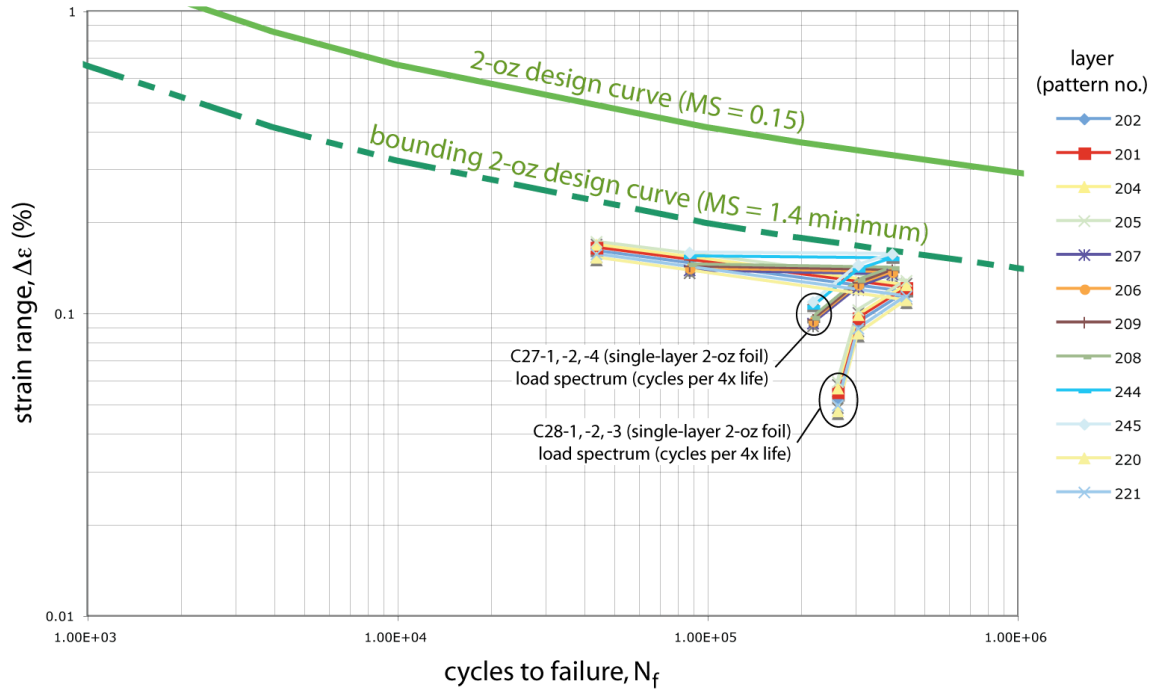


Figure 39. Strain-range spectra for the 2-oz omega flex cables with the redesigned C27-4 and C28-2.

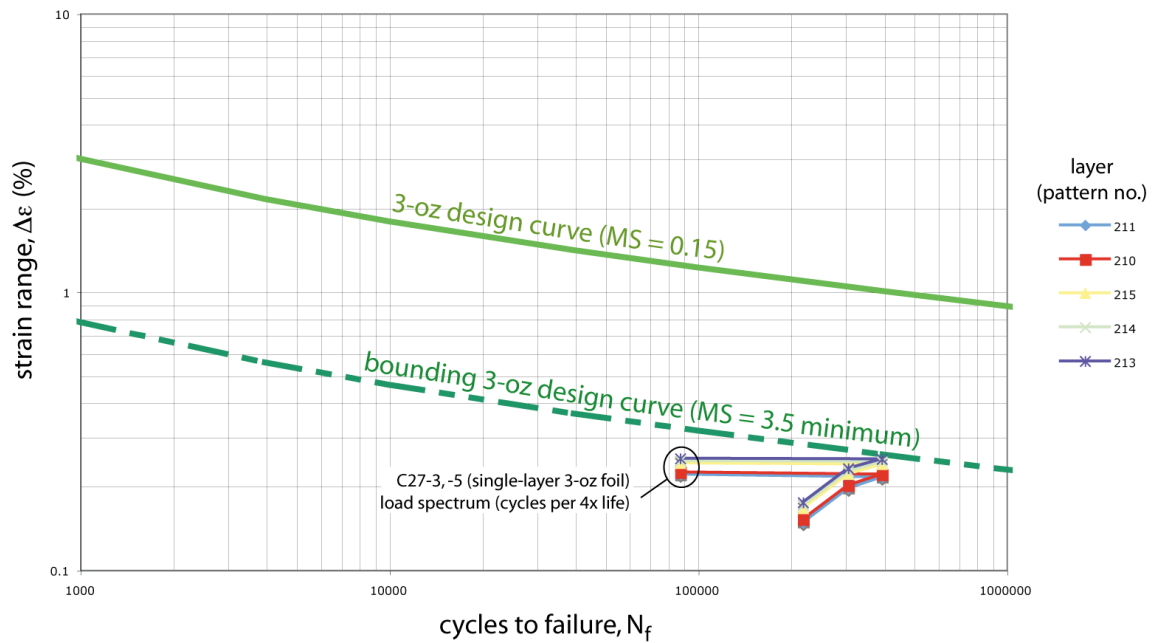


Figure 40. Strain-range spectra for the 3-oz omega flex cables under the new constraints set by the redesigned C27-4 cable.

2.4.2 Larger Bend Radius

A second alternative to dealing with the strains exhibited by the original C27-4 design would be to increase the plate-to-plate distance that constrains the cable (see Figure 7). However, in order to reduce the maximum strain-range spectrum down to where it is bounded by the 2-oz design curve, the constraint would have to be increased to ~6 inches. The impact that such a change would require on the surrounding azimuth mechanical assembly is beyond the scope of this paper.

2.4.3 Increase Ductility

If it remains desirable to retain a double-sided circuit design for the C27-4 cable (e.g., for EMI reasons), a possible solution for increasing design life would be to take advantage of the increased robustness of the 3-oz cables over the 2-oz designs (see Figure 35). Following the approach of §2.3, the load spectra for the resulting C27 cable set design is provided in Figure 41. As can be seen, the result would be just acceptable.

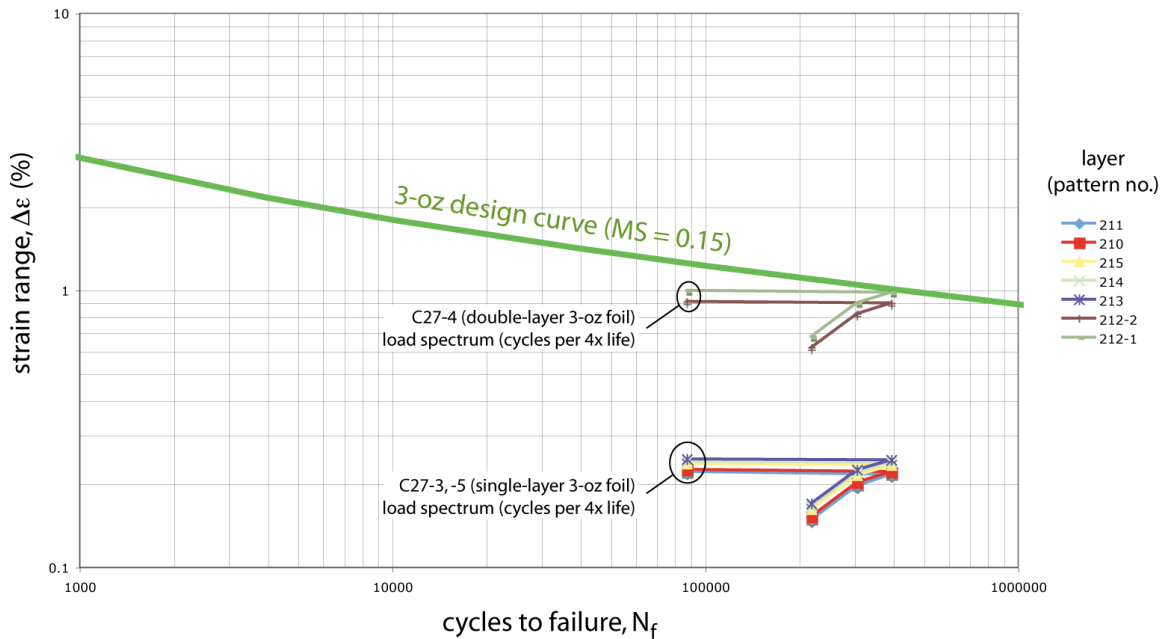


Figure 41. C27 cable set load spectra for 3-oz, double-layer C27-4 design.

Additional margin could be gained by altering the ground plane layer design to balance the location of the neutral strain plane (i.e., equivalent moment of inertia of areas for both circuit layers). Another possibility to investigate would be to use a design that reduces the

polyimide base (inter-copper dielectric) layer thickness (see Figure 4) by, for example, reducing Kapton film thickness from 2 mils to 1 mil and by eliminating two 1-mil thick Teflon layers (assuming this configuration is both producible and will provide adequate electrical performance).

3 Cable Qualification

Although not detailed out here for the case study, note that flex cable qualification plans should follow IPC-6013A with Amendment 2, *Qualification and Performance Specification for Flexible Printed Boards*, April 2006. Consideration may also be given to MIL-PRF-31032/3A with Amendment 1, *Performance Specification Sheet, Printed Wiring Board, Flexible, Single and Double Layer, With or Without Plated Through Holes, With or Without Stiffeners for Soldered Part Mounting*, 24 February 2006.

DISTRIBUTION:

1 MS0899 Technical Library, 9536 (electronic copy)



Sandia National Laboratories